Quinoline derivatives as Fluorescent Probes for Zinc Determination in Living Cells

Pavlo Virych

pavlo.virych@knu.ua

Taras Shevchenko National University of Kyiv

Sergey Studzinsky

Taras Shevchenko National University of Kyiv

Petro Virych

Institute of Otolaryngology named after Prof. A.I. Kolomiychenko of the National Academy of Medical Sciences of Ukraine

Nataliya Kutsevol

Taras Shevchenko National University of Kyiv

Oksana Krupka

University of Angers

Vitaliy Smokal

Taras Shevchenko National University of Kyiv

Research Article

Keywords: 8-Hydroxyquinolines, zinc sensing, ZnO nanoparticles, fluorescent probe, live-cell imaging

Posted Date: February 17th, 2026

DOI: https://doi.org/10.21203/rs.3.rs-8708964/v1

Additional Declarations: No competing interests reported.

Abstract

Fluorescence sensors are one of rapid technics for metal cation determination in cells, tissues and biological fluids. 8-Hydroxyquinoline (8HQ) derivatives have possess favorable photophysical and coordination properties for developing fluorescent metal sensors. 8HQ derivatives 2-(4-methoxystyryl)quinolin-8-ol (STQ-Me), 2-(4-ethoxyphenylethenyl)quinolin-8-ol (STQ-Et) and 2-(4-(trifluoromethyl)styryl)quinolin-8-ol (STQ-CF) were investigated. Absorbance and fluorescence spectra of 50 μM 8HQ derivatives in saline were evaluated in the presence of Mg, Ca, and Zn. The cytotoxicity was carried out on epidermal carcinoma of the mouth KB cell line. Fluorescence of KB cells, incubated for 5 h with ZnO nanoparticles, was measured after treatment with a 30 μM solution of the corresponding 8HQ derivative. N-(6-Methoxy-8-quinolinyl)-4-methylenebenzenesulfonamide (TSQ) served as a reference zinc indicator. Among the studied compounds, STQ-Me demonstrates sufficient stability in saline and appears to be able to bind Zn with presumably some selectivity in the presence of Ca and Mg. The fluorescence intensity of STQ-Me solution increased with rising Zn concentration in the presence of Ca and Mg. Compounds STQ-Et and STQ-CF demonstrated either weak divalent cation selectivity, poor stability and a pronounced tendency to aggregate in saline. In live KB cells incubated with ZnO NPs, STQ-Me produced a zinc-dependent fluorescence pattern similar to the reference probe TSQ. However, STQ-Me was likely unable to chelate protein-bound zinc, as evidenced by the dynamic fluorescence parameters of KB cells. Overall, STQ-Me demonstrates potential as a fluorescent probe for monitoring labile zinc in living cells, but further molecular optimization is required to enhance fluorescence output and improve binding to protein-associated zinc pools.

1 Introduction

Metals are involved in many physiological functions of cells. They are responsible for transmembrane potential, osmotic pressure, catalysis, protein stabilization, transport, etc. Metabolic dysfunctions are accompanied by changes in the cationic composition of blood and tissues [1–5]. The cation content changes in response to malignant transformation of cells, development of diabetes, disruption of hormone secretion and other pathologies. Ca^{2+}, Mg^{2+}, and Zn^{2+} are the most abundant divalent cations in the body. Magnesium plays an important role in the pathogenesis of the cardiovascular system and excitable tissues in general. Its content in tissues is the highest among divalent cations [6]. In addition, magnesium is involved in the metabolism of nucleic acids, energy production, enzymatic catalysis, cellular signaling, etc. [7]. Calcium is the second most abundant divalent cation. This element is involved in cell signaling, regulation of biochemical processes, proliferation, immune response, cell death, cell movement and as a structure-forming element of bones and the exoskeleton of invertebrates. The main calcium depo in the cell are mitochondria and the endoplasmic reticulum [8]. It should also be noted that the role of zinc, in addition to the other ions, is key in maintaining cellular homeostasis. Most disorders are accompanied by disruption in zinc homeostasis. Among them cancer progression and diabetes are the most studied [9].

Rapid metal cations determination is very important in diagnostics and prescribing treatment. Fluorescence detection is one of these methods. Fluorescence sensors bind to an accessible metal ion and change their optical properties. The phenomenon is accompanied by an increase in fluorescence or a change in the emission wavelength. Selectivity of cation binding is an important characteristic of fluorophores. 8-Hydroxyquinoline (8HQ) derivatives have the necessary set of properties for the creation of fluorescent metal cation sensors.

8HQ are known for its wide range of optical, chemical properties and biological effects [10–14]. Cation chelation is an important feature of these compounds in the creation of biologically active substances [15–17]. Metal complexes of 8HQ exhibit antibacterial and antiproliferative activity. 8HQ acts as fluorophoric ligand on complex formation with alkaline-earth and transition metal cations. It is considered as a building block in metallo-supramolecular chemistry for investigation of cations. 8HQ moiety is used as development fluorescent chemosensors in material, analytical and bioorganic chemistry, molecular imaging, medical and biological investigations [18]. One difficulty is the hydrophobicity of the 8HQ-derivative sensors. Aggregates interfere with accurate measurements of optical absorption or fluorescence in water solutions. However, poor solubility in water does not prevent the creation of new fluorescent chemosensors for cation detection [19, 20].

Selective determination of cations in living cells is difficult due to the multi-component mixture of organic and inorganic components. They interfere with chelation, distort the optical signal, or destroy the chemosensory molecule.

The aim was to determine the possibilities of chelation of calcium, magnesium and zinc by (8HQ) derivatives 2-(4-methoxystyryl)quinolin-8-ol (STQ-Me), 2-(4-ethoxyphenylethenyl)quinolin-8-ol (STQ-Et) and 2-(4-(trifluoromethyl)styryl)quinolin-8-ol (STQ-CF_3) separately and in a mixture based on physiological solution. The optical absorption and fluorescence of aqueous solutions of test molecules in the presence of cations was investigated. The cytotoxic properties of the substances were tested against epidermal carcinoma of the mouth KB cell line. The substance, most suitable for intracellular zinc measurements, was identified. The potential of this substance for studying dynamic changes in intracellular zinc was tested in comparison with the well-known fluorescent chemosensor N-(6-methoxy-8-quinolinyl)-4-methylenebenzenesulfonamide (TSQ).

2 Materials and methods

2.1 8-hydroxyquinoline derivatives

The derivatives from the condensation reaction of 8-hydroxy-2-methylquinoline (STQinit) and a series of benzaldehydes were prepared by modifying a previously described method [21]. The synthesis involved a condensation reaction in acetic anhydride (Ac_2O). The compounds 2-(4-methoxyethenyl)quinolin-8-ol, 2-(2-(4-ethoxyphenylethenyl)quinolin-8-ol and 2-(4-(trifluoromethyl)ethenyl)quinolin-8-ol were synthesized from their corresponding intermediary acetate precursors, 2-(4-methoxyethenyl)quinolin-8-yl acetate, 2-

(4-ethoxyphenylethenyl)quinolin-8-yl acetate, and and 2-(4-(trifluoromethyl)ethenyl)quinolin-8-yl acetate respectively. Synthetic route and chemical structures of the 8HQ derivatives compounds are shown in Fig. 1.

2-(4-methoxystyryl)quinolin-8-yl acetate

A flask was charged with a mixture of 8-hydroxy-2-methylquinoline (3 g, 18.9 mmol), 4-methoxybenzaldehyde (2.6 g, 18.9 mmol) and acetic anhydride (20 ml). The reaction mixture was heated at 140°C under reflux for 14 hours, with the progress monitored by TLC. Following the completion of the reaction and subsequent cooling of the mixture to room temperature, the reaction was quenched by adding ice-cold water to precipitate the product. The precipitated product was collected by filtration, washed repeatedly with water, and then dried. The crude product was subsequently purified by recrystallization from ethanol yield 62%. Mp 127–128˚C. ^{1}H NMR (400 MHz, DMSO-d6), δ, ppm: 2.50 (s, 3H, -CH_3), 3.8 (s, 3H, -OCH_3), 6.9–7.0 (d, 2H, Ar-H), 7.2–7.3 (d, 1H, =CH–), 7.4–7.5 (m, 2H, Het), 7.6 (d, 2H, Ar-H), 7.74–7.78 (d, 1H,=CH–), 7.8 (m, 2H, Het), 8.38 (d, 1H, Het),

2-(4-ethoxyphenylstyryl)quinolin-8-yl acetate

The same procedure as for 2-(4-methoxystyryl)quinolin-8-yl acetate was used with 4-ethylbenzaldehyde. The solid residue was recrystallized from ethanol, yield 80%. Mp 213–215˚C. ^{1}H NMR (400 Hz, DMSO-d6), δ, ppm: 1.4 (m, 6H, 2CH_3), 4.06–4.08 (m, 2H, -CH_2-), 6.9 (d, 2H, Ar–H), 7.1–7.2 (d, 1H, =CH–), 7.41–7.46 (m, 1H, Het; 1H, =CH–), 7.5 (d, 2H, Ar–H), 7.6–7.66 (m, 3H, Het), 8.08–8.1 (d,1H, Het).

2-(4-(trifluoromethyl)styryl)quinolin-8-yl acetate

The same procedure as for 2-(4-methylstyryl)quinolin-8-yl acetate was used with 4-ethylbenzaldehyde. The solid residue was recrystallized from ethanol, yield 80%. Mp 116–117˚C.

^{1}H NMR (400 Hz, DMSO-d6), δ, ppm: 2.5 (s, 3H, CH_3), 7.3–7.34 (d, 1H, =CH–), 7.36 (d, 2H, Ar–H), 7.43 (t, 1H, Het), 7.5–7.6 (m, 6H, Het; =CH–; Ar-H), 8.04 (d, 1H, Ar–H).

2-(4-methoxystyryl)quinolin-8-ol (STQ-OMe)

The solution of 2-(4-methoxystyryl)quinolin-8-yl acetate (3.5g, 10.1 mmol) in ethanol (100 ml) and concentrated hydrochloric acid (20 mL) was refluxed for 2h. The yellow precipitate was filtered and washed thoroughly with water. It was subsequently dissolved in ethanol (50mL) and triethylamine (17mL) was added and stirred at room temperature for 1h. The ice-cool water was added and the precipitate was filtered, washed with water and dried to afford 2-(4-methylstyryl)quinolin-8-ol. Compound was purified by recrystallization from ethanol. Yellow crystals, yield 69%. Mp 113–115˚C. ^{1}H NMR

(400Hz, $CDCl_3$), δ, ppm: 3.8 (s, 3H, -OCH_3), 6.92–6.94 (d, 2H, Ar-H), 7.13–7.15 (d, 1H, Het), 7.17–7.21 (d, 1H, =CH–), 7.26 (m, 1H, Het), 7.3 (t, 1H, Ar–H), 7.5–7.6 (m, 3H, Het), 7.63–7.67 (d, 1H, =CH–), 8.01 (d, 1H, Het), 09.15 (s, 1H, –OH).

2-(4-ethoxyphenylethenyl)quinolin-8-ol (STQ-OEt)

The same procedure as for 2-(4-methoxystyryl)quinolin-8-ol was used, yield 75%. Mp 120 ˚C. ^{1}H NMR (400Hz, DMSO-d6), δ, ppm: 1.4 (m, 3H, CH_3), 4.04–4.06 (m, 2H, –CH_2–), 6.9 (d, 2H, Ar–H), 7.0 (d,1H, –CH=), 7.2–7.3 (m, 2H, Ar–H; 1H, –CH=), 7.5 (d, 2H, Ar–H), 7.6 (d, 1H, Ar–H), 7.9 (d, 1H, Ar–H), 8.13–8.15 (d,1H, Ar–H), 9.09 (s, 1H, –OH).

2-(4-(trifluoromethyl)styryl)quinolin-8-ol (*STQ-CF_3)*

The same procedure as for 2-(4-methylstyryl)quinolin-8-ol was used, yield 95%. Mp 136 ˚C. ^{1}H NMR (400 Hz, DMSO-d_6), δ, ppm: 7.10 (d, 1H, Ar–H), 7.23 (d, 1H, Ar–H), 7.38–7.42 (m, 1H, –CH=; m, 1H, Ar–H), 7.60–7.63 (d, 1H, –CH=), 7.65–7.73 (m, 4H, Ar–H; m, 1H, Ar–H), 8.08 (s, 1H, –OH), 8.10–8.12 (d, 1H, Ar–H).

2.2 Cation chelation and time stability

A 50 mM solution of 8HQ derivatives STQ-Me, STQ-Et and STQ-CF_3 based on DMSO were prepared. An aliquot of the stock solution was added to saline. The final concentration was 50 μM. The optical absorption spectra at wavelength 230–500 nm were recorded (PerkinElmer Lambda 365 UV, Waltham, Massachusetts, USA) The absorbance was measured immediately after the addition of 8HQ derivatives, as well as after 5, 20, 40 and 60 min.

Stock solutions 50 mM of Ca^{2+} ($CaCl_2$), Mg^{2+} ($MgCl_2$) and Zn^{2+} ($Zn(CH_3COO)_2$ were prepared in saline. A solution of each cation and their mixture in equal molar ratio (Ca^{2+}: Mg^{2+}:Zn^{2+} = 1:1:1) was prepared in the concentration range of 500 − 7.8 μM by the two-fold dilution method. An aliquot of the corresponding 8HQ derivative (STQ-Me, STQ-Et, STQ-CF_3) was added to each solution. The final concentration was 50 μM. Absorbance was measured on a Perkin Elmer Lambda 365 UV spectrophotometer in the wavelength range of 230–500 nm after 0, 5, 20, 40, and 60 min. Measurements were carried out in 10x10x40 mm quartz cuvettes at room temperature.

The molar extinction coefficient (ε) was calculated by Law Bouguer-Beer-Lambert from the absorbance maxima of the tested 8HQ derivatives. The measurements were repeated four times.

2.3 Fluorescence investigation

Fluorescence was measured using a Shimadzu RF-6000 spectrofluorophotometer (Shimadzu, Kyoto, Japan). The fluorescence of STQ-Me (50 μM) and STQ-Et (50 μM) in saline was recorded at excitation wavelengths corresponding to the main absorbance maximum (390 nm) and the secondary maximum

(280 nm). The fluorescence of STQ-CF_3 (50 μM) was registered at excitation wavelengths of 300 and 360 nm. 8HQ derivatives in saline (50 μM) were incubated for 40 min with the corresponding cation or cation mix. The cation concentrations were 15.625, 31.25, 62.5, and 500 μM. Measurements were carried out in 10x10x40 mm quartz cuvettes at room temperature. The fluorescence of STQ-Me and STQ-Et was recorded at excitation wavelength 280 nm, and STQ-CF_3 was measurement at 360 nm. As an additional indicator, the ratio of the fluorescence amplitude of the initial 8HQ derivative solution (F_c) to that in the presence of the corresponding cation(s) (F_s) was calculated. The measurements were repeated four times.

2.4 Cytotoxycity

The research was carried out on epidermal carcinoma of the mouth KB cell line. Cells were incubated in 96-well plates in DMEM medium (Biowest, Nuaillé, France), 10% bovine serum (Biowest), 40 μg/ml gentamicin and an atmosphere of 5% CO_2 at 37°C. 8HQ derivatives in DMSO were added to the incubation solution by the method of two-fold dilutions at the concentration range of 500 – 7.8 μM. After 24 h, the medium was removed. Cells were stained with 50 μl crystal violet (5 mg/ml in 70% methanol) for 10 min. Wells were washed three times with distilled water. The number of cells was determined photometrically on a tablet spectrophotometer at 540 nm. The study was repeated four times. Data were present as mean and standard deviation (m ± SD).

2.5 Zinc measurement in cells

KB cells were grown on glass coverslips in DMEM (Biowest) supplemented with 10% bovine serum (Biowest) and 40 μg/mL gentamicin in a 5% CO_2 atmosphere at 37°C for 48 h. The dextran-co-polyacrylamide/ZnO nanoparticles nanosystem (DPAA/ZnO NPs) was used to deliver zinc into KB cells. Detailed specifications of the nanosystem were published earlier [23, 24]. ZnO NPs were used to induce larger fluctuations in intracellular zinc levels compared to zinc salt solutions. This is due to the activation of cellular defense mechanisms for Zn^{2+} efflux [9]. The nanosystem was added to the incubation solution and thoroughly mixed. The concentration of DPAA/ZnO NPs in the incubation solution was 2 mM. Intracellular zinc levels were measured every 15 min during the first hour of incubation and then hourly for up to 5 h. When the required time period was passed, the coverslips with the KB cells were washed in saline for 30 s. An aliquot of a 50 mM stock solution of STQ-Me, STQ-Et, or STQ-CF_3 in DMSO was added to phosphate-buffered saline (PBS, Biowest). The final concentration of 8HQ derivatives was 30 μM. The reference fluorescent zinc indicator N-(6-methoxy-8-quinolinyl)-4-methylenebenzenesulfonamide (30 μM in PBS, TSQ, Sigma-Aldrich, USA) was used [25]. KB cells were incubated with the respective 8HQ derivative for 30 min. Coverslips with KB cells were washed in saline for 30 min. Fluorescence was registered using an Olympus BX53 (Tokyo, Japan) microscope equipped with an XCite Series 120 Q fluorescent block and an Olympus DP72 camera. Fluorescence excitation was performed by an ultraviolet light filter, whereas emission was collected by a blue/green light filter (STQ-Me, STQ-Et, TSQ) and blue/red light filter (STQ-CF_3). Exposure was 10 ms for TSQ and 20 ms for investigated 8HQ derivatives. At least 20 fields of view were snapped for each sample. Testing and

luminescence registering were performed under the same conditions for all cells. Cell images processing was carried out with the ImageJ software (Bethesda, Maryland, USA). Integrate density of 50 individual cells was measured for each sample. Experiments were carried out in triplicate. Kruskal-Wallis test was used to compare the non-parametric data. The difference was statistically significant at $p < 0.05$. Data were presented as the median and interquartile range (median (Me), 25–75%).

3 Results and discussion

3.1 Cation chelation and time stability

8HQ derivatives exhibit poor solubility in aqueous solutions. 50 μM solutions of STQ-Me, STQ-Et, and STQ-CF_3 were prepared in saline. The absorbance spectra in the range 230–500 nm were changed over time (Fig. 2a). The highest absorbance intensity was recorded for the 50 μM STQ-Me solution. Absorbance was increased over time and reached a peak after 20 min of incubation. It was suggested that such behavior was related to the compound dissolution process. No similar effects were observed for STQ-Et (Fig. 2b).

Maximum absorbance was recorded for the initial solutions and decreased over time. These indicators were evidence of aggregation processes. The poorest absorbance characteristics were identified for the aqueous solution of STQ-CF_3 (Fig. 2c). Very slight changes in absorbance amplitude over time were recorded.

The molar extinction coefficients (ε) at the absorbance maxima were calculated (Table 1).

Table 1
Molar extinction coefficients of 50 μM solutions of STQ-Me, STQ-Et, and STQ-CF_3 in saline over time

Time	STQ-Me			STQ-Et			STQ-CF_3
	ε, $L \cdot Mol^{-1} \cdot cm^{-1}$			ε, $L \cdot Mol^{-1} \cdot cm^{-1}$			ε, $L \cdot Mol^{-1} \cdot cm^{-1}$
	267 nm	322 nm	392 nm	270 nm	321 nm	397 nm	360 nm
0 min	9540	13320	23500	6360	8460	12540	3460
5 min	10840	15120	28340	6360	8460	12320	3680
20 min	11700	16660	31260	6360	8460	11960	3680
40 min	12200	16980	32320	5740	7640	11100	4180
60 min	12200	16980	32320	5740	7640	10800	4360

At the absorbance spectra of the STQ-Me were identified three maxima at 267 nm, 322 nm and 392 nm. An increase in the ε of the main maximum at 392 nm by 1.4-fold was recorded over 60 min. This indicator was increased by 1.3-fold at the secondary maxima of 267 nm and 322 nm. The difference

between ε at the main maximum at the initial time point (0 min) for STQ-Me (392 nm) and STQ-Et (397 nm) was 1.9-fold. However, minimal changes in the indicator were observed over time for STQ-Et, in contrast for STQ-Me. A 10–15% decrease in the ε was identified after 60 min relative to the initial values for STQ-Et. A single well-defined optical absorption maximum at 360 nm was detected in the spectrum of STQ-CF_3. The molar extinction coefficient (0 min) was decreased by 6.8-fold compared to STQ-Me and by 3.6-fold compared to STQ-Et. The results for this compound were the worst compared to other samples. Presumably, STQ-CF_3 had the lowest solubility in aqueous solutions.

Although it is well known that simple quinoline is a monodentate ligand, its derivatives are often far more interesting because they can act as chelating agents (bidentate ligands). This has been confirmed in a number of works where 8HQ derivatives have coordinating ability, which allows them to be used for metal chelation [26]. Ca^{2+}, Mg^{2+}, and Zn^{2+} are the most abundant divalent cations in cells. The ability of 8HQ derivatives to chelate these cations in saline was tested. The concentration of 8HQ derivatives was constant in all test solutions and equal to 50 μM. Stock solutions 50 mM of Ca^{2+} ($CaCl_2$), Mg^{2+} ($MgCl_2$) and Zn^{2+} ($Zn(CH_3COO)_2$) were prepared in saline. The concentrations of each cation were varied to achieve 8HQ:cation ratios of approximately 3:1, 2:1, 1:1, and 1:10. A significant decrease in the absorbance of STQ-Me solutions was registered in the presence of Mg^{2+} (Fig. 3a).

Changes in the absorbance spectra were dependent on the ratio of Mg^{2+} to STQ-Me. The highest absorbance intensity at the main maximum was registered at STQ-Me : Mg^{2+}ratios of 1:2 and 1:1. All other ratios resulted in decreased absorbance. The increased absorbance at these ratios suggests that the chelation of Mg^{2+} stabilizes the dye's excited state or prevents self-quenching aggregation. It was suggested that chelation with Mg^{2+} occurs optimally at a ratio of 2 STQ-Me molecules to 1 cation. In this case, the solubility of the formed Mg^{2+} complex is also likely reduced compared to that of free STQ-Me. Less significant changes in the absorbance spectra of STQ-Me were registered in the presence of Ca^{2+} (Fig. 3b). The lowest absorbance amplitude of the main maximum was determined at a STQ-Me : Ca^{2+} ratio of 3:1. An increase in the absorbance was observed both with a large excess of calcium and at lower Ca^{2+} concentrations corresponding to STQ-Me : Ca^{2+} ratios of 2:1 and 1:1. The absorbance spectra of STQ-Me in saline were changed in a concentration-dependent manner in the presence of Zn^{2+} (Fig. 3c). Similar data were obtained when studying the absorbance spectra STQ-Me in the presence of Ca^{2+}, Mg^{2+} and Zn^{2+} (Fig. 3d).

It has been suggested that these results indicate a preferential chelation of Zn^{2+} than Mg^{2+} and Ca^{2+}. The molar extinction coefficients of the STQ-Me solutions with the three cations were exhibited changes analogous to those observed with Zn^{2+}, though they were not strictly corresponded. (Table 2).

Table 2

Molar extinction coefficients of 50 μM solutions of STQ-Me in presence of Mg^{2+}, Ca^{2+} and Zn^{2+} in saline

Cation concentration, μM	STQ-Me, 5 min			
	Mg^{2+}, ε (392 nm), $L \cdot Mol^{-1} \cdot cm^{-1}$	Ca^{2+}, ε (392 nm), $L \cdot Mol^{-1} \cdot cm^{-1}$	Zn^{2+}, ε (392 nm), $L \cdot Mol^{-1} \cdot cm^{-1}$	Mg^{2+}, Ca^{2+}, Zn^{2+}, ε (392 nm), $L \cdot Mol^{-1} \cdot cm^{-1}$
0	23500			
15.625	9480	13680	14860	12720
31.25	12520	19860	10240	12220
62.5	11320	25280	9220	10200
500	7820	16440	8140	8040

Presumably, a mixture of STQ-Me–Me^{2+} complexes with various cations was formed, the majority of which contained Zn^{2+}. The change in the absorbance intensity of STQ-Me solutions in the presence of Mg^{2+}, Ca^{2+} and Zn^{2+} was assessed over a period of 60 min. Cation concentrations corresponding to the maximum absorbance amplitude at the main maximum for STQ-Me : cation ratio was selected (Fig. 4).

A time-dependent increase in the absorbance of STQ-Me in saline was observed with the addition of Ca^{2+} and Mg^{2+} (Fig. 4a, b). In the presence of Mg^{2+}, the indicator continued to increase up to 60 min. In the presence of Ca^{2+}, the absorbance amplitude increased over the first 20 min and then remained constant up to 60 min. Thus, the formed STQ-Me–Ca^{2+} and STQ-Me–Mg^{2+} complexes require some time for both chelation and stabilization in aqueous solution to achieve a state of equilibrium. In contrast, the absorbance amplitude of STQ-Me solutions in the presence of Zn^{2+} was stabilized after 5 min and remained unchanged thereafter (Fig. 4c). It is important to note that the observed time-dependent changes in the absorbance spectra of STQ-Me solutions with individual Mg^{2+}, Ca^{2+}, and Zn^{2+} likely do not indicate significant aggregation processes after equilibrium is established. The absorbance amplitude of STQ-Me aqueous solutions containing a mixture of cations was decreased after 20 min of incubation (Fig. 4d). Thus, the binding processes and stability of the complexes of STQ-Me in saline with individual Mg^{2+}, Ca^{2+}, Zn^{2+} and in their mixtures were different.

A decrease in the absorbance intensity at the main maximum of the STQ-Et solution was identified at chelator : cation ratios of 2:1 and 1:1 following the addition of Mg^{2+} (Fig. 5a). No significant changes in this parameter were observed with either low or excess concentrations of Mg^{2+} in the saline. The amplitude of the main absorbance maximum of STQ-Et was significantly reduced in the presence of Zn^{2+}, Ca^{2+}, and the cation mix (Fig. 5b, c, d).

This parameter was weakly dependent on the cation concentration. The molar extinction coefficient decreased by approximately 40–60% (Table 3).

Table 3

Molar extinction coefficients of 50 μM solutions of STQ-Et in presence of Mg^{2+}, Ca^{2+} and Zn^{2+} in saline

Cation concentration, μM	STQ-Et, 5 min			
	Mg^{2+}, ε (397 nm), $L \cdot Mol^{-1} \cdot cm^{-1}$	Ca^{2+}, ε (397 nm), $L \cdot Mol^{-1} \cdot cm^{-1}$	Zn^{2+}, ε (397 nm), $L \cdot Mol^{-1} \cdot cm^{-1}$	Mg^{2+}, Ca^{2+}, Zn^{2+}, ε (397 nm), $L \cdot Mol^{-1} \cdot cm^{-1}$
0	12540			
15.625	10760	7780	7040	7020
31.25	8460	5920	7440	6040
62.5	7700	6620	8080	8080
500	11480	6540	5760	6720

It is also important to note that the peak at 270 nm was almost smoothed out. Therefore, STQ-Et showed no concentration-dependent changes in its absorbance spectra in the presence of Ca^{2+}, Zn^{2+}, or cation mix. No evidence of selective chelation by STQ-Et of divalent cations was identified.

Minor time-dependent changes in the absorbance spectra of STQ-Et saline solutions with Mg^{2+}, Ca^{2+}, and Zn^{2+} were detected (Fig. 6). The most significant decrease in the amplitude of the main maximum at 397 nm was 13% over 60 min for STQ-Et with Mg^{2+} (Fig. 6a). In the presence of Zn^{2+}, the main maximum remained unchanged over time, but an increase in the absorbance at the secondary maximum of 321 nm was identified (Fig. 6c). This phenomenon was not observed in solutions containing a mix of Mg^{2+}, Ca^{2+}, and Zn^{2+} (Fig. 6d).

Visibly detectable aggregates of STQ-CF_3 were observed after its addition to saline. The solubility of this compound in aqueous solutions and the stability of its suspensions was poor. Accordingly, the optical absorbance of such solutions was low. However, an increase in the optical absorbance of STQ-CF_3 solutions was detected in the presence of Mg^{2+}, Ca^{2+}, Zn^{2+}, or their mix (Fig. 7).

As with STQ-Me, a correlation was identified between the absorbance spectra of STQ-CF_3 aqueous solutions and the concentration of cations. The amplitude of the main absorbance maximum at 360 nm was highest at a STQ-CF_3 : Mg^{2+} ratio of approximately 1:1 (Fig. 7a).

Both increase and decrease this ratio resulted in a slight drop in optical absorbance. No similar changes were observed in the presence of Ca^{2+} or Zn^{2+} (Fig. 7b, c). The optical absorbance of STQ-CF_3 solutions was not dependent on the concentration of divalent cations in the mix (Fig. 7d).

The calculated molar extinction coefficients at the main maxima were increased by 2.5-3-fold for STQ-CF_3 solutions in the presence of divalent cations compared to those without cations (Table 4). For STQ-CF_3, ε was independent of the concentration of Ca^{2+}, Zn^{2+}, or the cation mixture.

Table 4
Molar extinction coefficients of 50 μM solutions of STQ-CF_3 in presence of Mg^{2+}, Ca^{2+} and Zn^{2+} in saline

Cation concentration, μM	**STQ-CF_3, 5 min**			
	Mg^{2+}, ε (360 nm), $L \cdot Mol^{-1} \cdot cm^{-1}$	**Ca^{2+}, ε (360 nm), $L \cdot Mol^{-1} \cdot cm^{-1}$**	**Zn^{2+}, ε (360 nm), $L \cdot Mol^{-1} \cdot cm^{-1}$**	**Mg^{2+}, Ca^{2+}, Zn^{2+}, ε (360 nm), $L \cdot Mol^{-1} \cdot cm^{-1}$**
0	3460			
15.625	7600	8080	9480	8780
31.25	8180	7720	9120	8560
62.5	9420	7180	9480	8240
500	6500	7280	7140	7660

As already mentioned, aqueous solutions of STQ-CF_3 were very unstable and prone to aggregation. Based on this, the optical absorbance spectra were also dependent on the degree of mixing and the presence of large aggregates. However, an increase in absorbance at 360 nm was detected within 60 min in STQ-CF_3 solutions with Mg^{2+}, Ca^{2+}, and Zn^{2+} (Fig. 8a, b, c).

The mixture of cations promoted even stronger aggregation of STQ-CF_3. Therefore, the absorbance spectra of these solutions over time became more chaotic and dependent on the degree of aggregation (Fig. 8d).

8HQ derivatives are used as chemosensors for the determination of cation and cationic ions in solutions [18, 20]. Detection is based on changes in the color or fluorescence of the solutions. Based on the results, the compound STQ-Me demonstrates sufficient stability in saline and appears to be able to bind Zn^{2+} with presumably some selectivity in the presence of Ca^{2+} and Mg^{2+}. The compounds STQ-Et and STQ-CF_3 demonstrated either weak divalent cation selectivity or very poor stability and a tendency to aggregate in saline. However, the induction of aggregation in metal complexes of 8HQ derivatives is also employed as a method for zinc detection [19]. The 8HQ derivatives STQ-Me and STQ-Et lack the

necessary properties for this cation detection method, while STQ-CF_3 is aggregated in aqueous solutions.

3.2 Fluorescence investigations

Fluorescence of STQ-Me, STQ-Et, and STQ-CF_3 in saline was carried out in the presence of Mg^{2+}, Ca^{2+}, and Zn^{2+}. The results of the time stability assessment showed that, after 40 min of incubation, almost all samples had reached an equilibrium state. That is why all solutions were held for 40 min before fluorescence measurements. Fluorescence excitation for the compounds STQ-Me and STQ-Et was carried out at the main absorbance maximum of 360 nm and the secondary maximum of 280 nm. The concentration of 8HQ derivatives in saline was 50 μM. The fluorescence maxima were identified at 560 nm for STQ-Me and STQ-Et after excitation (Ex) with 280 nm light (Fig. 9a).

The fluorescence amplitude for STQ-Et was 20% higher than that of STQ-Me. Excitation of solutions of these compounds at 390 nm induced fluorescence with a maximum at 520 nm, but with an intensity 20–30 times lower (Fig. 9b). The noted high-intensity fluorescence bands (with a maximum at 520 nm) probably occur due to the emission of luminescent aggregates formed by the molecules of the studied styrylquinolines, the spectral properties of which are determined by the splitting of the corresponding energy levels upon association of the dyes. Such aggregates can be, in particular, fluorescent sandwich-type dimers (H-like aggregates) with a partially allowed low-energy exciton transition, as well as higher order associates [27]. The higher fluorescence yield of the aggregates may be due to the permittivity of the low-energy exciton transition (partial removal of the prohibition), which is caused by the larger angle between the dipole moments of the aggregates' monomer units during excitation. Due to the fixation of styrylquinoline molecules inside the aggregate, as well as the splitting of their electronic levels, each of them (levels) has a smaller number of vibrational sublevels, which leads to a shortening of the corresponding electronic-vibrational progression, and therefore to a weakening of vibronic interactions. As a result, the emission band of the aggregate is narrower compared to the emission band of the monomeric dye [27–32]. This conclusion is indirectly confirmed by the narrowness and lack of fine structure of the indicated luminescence bands, as well as by the fact that for a number of STQ-Me and STQ-Et-comparable compounds, the monomer luminescence bands corresponding to both short-wavelength (~ 280 nm) and long-wavelength (~ 390 nm) excitation are structured and may consist of several separate bands. In addition, for such compounds the ratio of the intensity of the long- and short-wavelength monomer fluorescence bands is significantly lower than in the studied case. An excitation wavelength of 280 nm was selected for further fluorescence investigations of the interactions between STQ-Me and STQ-Et with Mg^{2+}, Ca^{2+}, and Zn^{2+}. A pronounced red shift in the fluorescence of STQ-CF_3 in saline was identified (Fig. 9c). Two maxima were found at 603 nm after excitation at 300 nm and 723 nm after excitation at 360 nm. The noted spectral features also indicate the decisive influence of the STQ-CF_3 compound aggregation on the luminescent properties of its solutions, as follows from the simple excitonic model of electronic oscillators interaction [29, 33, 34], which is successfully applied to the absorption and fluorescence spectra of dye associates [27, 29, 34]. The fluorescence amplitude of STQ-CF_3 was 5–6 times higher than that of STQ-Me and STQ-Et at the same concentrations. It is important to

note that the fluorescence intensity of STQ-CF_3 was nearly independent of the excitation wavelength. Also, the fluorescence of 8HQ derivatives depends on intramolecular rearrangements and protonation/deprotonation [35, 36].

Fluorescence of aqueous solutions of 8HQ derivatives was measured after 40 min of incubation with the corresponding divalent cation. This duration was optimal for solution equilibration and the formation of 8HQ-Me complexes. A 1.5-1.8-fold decrease in the fluorescence of STQ-Me solutions was observed after the addition of Mg^{2+} (Fig. 10a, Table 5).

Nevertheless, the fluorescence amplitude showed a weak dependence on Mg^{2+} concentration. Slightly higher fluorescence was identified in STQ-Me solutions with Mg^{2+} concentrations of 15.625 µM and 500 µM. The absorbance amplitude was lowest in these solutions. Similar fluorescence results were obtained after the addition of Ca^{2+} to the solution (Fig. 10b). A decrease in fluorescence amplitude of 1.4–1.6 times was calculated (Table 5). A concentration-dependent increase in the fluorescence of STQ-Me solutions in the presence of Zn^{2+} was observed (Fig. 10c). These data are consistent with the trends observed in the absorbance changes of the same solutions. Similar concentration-dependent changes in fluorescence were observed after the addition of the Mg^{2+}, Ca^{2+}, and Zn^{2+} mixture, although the fluorescence amplitude varied (Fig. 10d).

Table 5
The ratio of the fluorescence amplitude of the initial 50 µM solution of STQ-Me (F_c) and in the presence of Mg^{2+}, Ca^{2+} and Zn^{2+} (F_s) in saline

Cation concentration, µM	Fluorescence F_c/F_s*, STQ-Me, 40 min			
	Mg^{2+}	Ca^{2+}	Zn^{2+}	Mg^{2+}, Ca^{2+}, Zn^{2+}
15.625	1.65	1.40	0.68	1.25
31.25	1.79	1.55	0.59	0.83
62.5	1.79	1.58	0.57	0.63
500	1.46	1.62	0.50	0.27

*F_c – fluorescence STQ-Me in saline; F_s – fluorescence STQ-Me in saline with divalent cation (s).

These results suggest that selective chelation of zinc most presumably occurs, although complexes with other divalent cations are also present in the solution. It is important to note that changes in the fluorescence of STQ-Me in the presence of Zn^{2+} occur in the opposite direction compared to those with Ca^{2+} and Mg^{2+} (Table 5).

Differences in fluorescence of STQ-Et solutions with divalent cations relative to STQ-Me were identified (Fig. 11).

The fluorescence of STQ-Et was decreased by 1.8-fold in the presence of excess magnesium (500 µM) (Fig. 11a, Table 6). The fluorescence amplitude slightly increased at the STQ-Et : Mg^{2+} ratio of 3:1 and 1:1 relative initial level. The optimal chelator : Mg^{2+} ratio was determined to be approximately 2:1. Similar results were observed following the addition of Ca^{2+} to the incubation solution (Fig. 11b). Optimal ratios of STQ-Et : calcium 1:1 and 3:1 with the highest fluorescence of solutions were identified. A 1.8-fold increase in fluorescence amplitude relative to the initial value was calculated. The fluorescence of STQ-Et solutions was increased after the addition of Zn^{2+} (Fig. 11c). Nearly identical fluorescence intensities of STQ-Et were observed in solutions containing Zn^{2+} at concentrations of 62.5 µM and 500 µM (Table 6). These dependencies were not found for the Mg^{2+}, Ca^{2+} and Zn^{2+} mix (Fig. 11d).

Table 6
The ratio of the fluorescence amplitude of the initial 50 µM solution of STQ-Et (F_c) and in the presence of Mg^{2+}, Ca^{2+} and Zn^{2+} (F_s) in saline

Cation concentration, µM	Fluorescence F_c/F_s*, STQ-Et, 40 min			
	Mg^{2+}	Ca^{2+}	Zn^{2+}	Mg^{2+}, Ca^{2+}, Zn^{2+}
15.625	0.86	0.53	0.72	0.83
31.25	0.79	0.63	0.96	0.43
62.5	0.87	0.55	0.62	0.40
500	1.76	1.88	0.64	0.56

*F_c – fluorescence STQ-Et in saline; F_s – fluorescence STQ-Et in saline with divalent cation (s).

These findings indicate that chelation was probably less selective compared to STQ-Me. Also, the STQ-Et complexes were characterized by other physical and chemical properties in aqueous solutions compared to STQ-Me. These properties were reflected in both absorption and fluorescence spectral changes, depending on the concentration of divalent cations.

A significant decrease in fluorescence was recorded at an STQ-CF_3 : Mg^{2+} ratio of 2:1 (Fig. 12a).

For other ratios, a 20–25% decrease in fluorescence relative to the initial level was found. The fluorescence amplitude of STQ-CF_3 decreased by 2-3-fold in the presence of Ca^{2+} concentrations exceeding 15.625 µM (Fig. 12b, Table 7).

Table 7
The ratio of the fluorescence amplitude of the initial 50 μM solution of STQ-CF_3 (F_c) and in the presence of Mg^{2+}, Ca^{2+} and Zn^{2+} (F_s) in saline

Cation concentration, μM	Fluorescence F_c/F_s*, STQ-CF_3, 40 min			
	Mg^{2+}	Ca^{2+}	Zn^{2+}	Mg^{2+}, Ca^{2+}, Zn^{2+}
15.625	1.30	1.18	1.79	1.43
31.25	2.83	3.23	1.49	1.58
62.5	1.17	2.53	2.07	0.82
500	1.30	1.87	0.64	1.24

*F_c – fluorescence STQ-CF_3 in saline; F_s – fluorescence STQ-CF_3 in saline with divalent cation (s).

An increase in fluorescence of the aqueous STQ-CF_3 solution by 1.6-fold was observed only in the presence of excess Zn^{2+} (500 μM) (Fig. 12c). The fluorescence patterns of STQ-CF_3 in a solution of cation mix were not as those for individual cation (Fig. 12d). Thus, this compound is not well suited for identifying divalent cations in aqueous solutions.

3.3 Cytotoxicity and fluorescence investigations in vitro

Some 8-HQ derivatives exhibit cytotoxicity against cancer cells [37], bacteria [38], viruses [39], and fungi [40]. The cytotoxicity of STQ-Me, STQ-Et, STQ-CF_3 in concentration range 7.8–500 μM against epidermal carcinoma of the mouth KB cell line was evaluated. A maximum cell death of approximately 25% for STQ-Et and 40% for STQ-Me was identified at a concentration of 62.5 μM (Fig. 13). This value was not changed with further concentration increase.

No cytotoxicity of the STQ-CF_3 was detected against the KB cell line in concentrations range 7.8–500 μM. Thus, no significant cytotoxicity of the investigated compounds was found.

To assess the potential use of 8HQ derivatives as fluorescent indicators for zinc detection, a model involving loading KB cells with ZnO NPs was selected. In previous studies, the dynamic loading parameters of the DPAA/ZnO NPs system into different cells were investigated using TSQ [24]. Based on those data, similar studies were carried out for the compounds STQ-Me, STQ-Et and STQ-CF_3. TSQ was used as a reference fluorescent indicator of intracellular zinc. A statistically significant increase in intracellular zinc levels was identified after 30 min of incubation with DPAA/ZnO NPs (Fig. 14a, Supplementary information (SI) – Fig. S1). The maximum values of the indicator were reached after 45 min and remained stable at this level for up to 2 h. A trend towards a decrease in intracellular zinc levels was recorded from 3 h incubation. The initial zinc level was restored after 5 hours of KB cell incubation with DPAA/ZnO NPs (Fig. 14a). The baseline integrated density of KB cells after staining with TSQ was 25 200 a.u. (median). The maximum values were calculated after 1 h of incubation and was 47 200 a.u

(median). The baseline integral density of KB cells after staining with TSQ-Me was 9 800 a.u., which was 2.5 times less than similar indicators for TSQ (Fig. 14b). It is important to note that the fluorescence of cells stained with the investigated 8HQ derivatives was recorded using a two-fold increase in exposure time. The maximum level of cell fluorescence (17,800 a.u.) was recorded after 30 min of incubation. Fluorescence was restored to its original values after 2 h (Fig. 14b).

No significant changes in baseline fluorescence of KB cells were observed after STQ-Et staining during incubation with DPAA/ZnO NPs. Fluorescence increased after 15 min of incubation and began to be restored after 30 min (Fig. 14c). No changes in cell fluorescence were identified after STQ-CF_3 staining and incubation with DPAA/ZnO NPs for 5 h. Fluorescent aggregates of STQ-CF_3 were identified between cells (SI – Fig. S2).

It is assumed that the increase in cell fluorescence after staining with STQ-Me and STQ-Et during short incubation times (15–30 minutes) is associated with the accumulation of ZnO NPs in vesicles and/or on the cell surface. In addition, a change in fluorescence color from blue to yellow was observed for these compounds (SI – Fig. S3, S4). This effect may be attributed to the potential for photostereoisomerization, as well as photoinduced proton transfer (for example, it is known that the pKa of 2styrylquinoline fragment significantly increases when excited by light from the ground (S_0) to the lowest excited singlet (S_1) state. And moreover, 2-styrylquinoline fragment is a photobase [41], so, the changes in fluorescence can be explained by metal ion photorecoordination or photochemical degradation processes in the intracellular medium. During these processes, the absorbance and fluorescence spectra undergo changes in response to light exposure [41–43]. In particular, some styrylquinoline dyes demonstrate multicolor fluorescence upon addition of different metal cations [44]. Interaction with proteins and other cellular polymers or low-molecular compounds cannot be ruled out either. It is important to note that this effect was observed for cells but was not detected in fluorescence studies carried out in saline.

Zinc in cells is almost absent as a free cation and is predominantly bound to proteins [9]. The fluorescent indicator TSQ binds to zinc regardless of its localization, including in proteins [45]. These properties enable the assessment of the total intracellular zinc level, irrespective of its chemical form. Therefore, the dynamic fluorescence change curve was not decreased after intracellular dissociation of ZnO NPs. The compound STQ-Me is most likely able to chelate of free zinc cations and forms available for binding, such as nanoparticles. But when zinc is deposited in proteins, it ceases to be available for STQ-Me. Due to this effect, cell fluorescence begins to decrease after ZnO NPs dissociation, Zn^{2+} release and their deposition on proteins.

Based on the results, the 8HQ derivatives STQ-Et and STQ-CF_3 were found unsuitable for assessing zinc levels in living cells. STQ-Me shows potential for measuring zinc levels in living cells. However, the molecule’s design requires further investigation and modification to enable chelation of protein-bound zinc and enhance fluorescence.

4 Conclusions

Based on the results, the compound STQ-Me demonstrates sufficient stability in saline and it seems to be able to bind Zn^{2+} with presumably some selectivity in the presence of Ca^{2+} and Mg^{2+}. Fluorescence of STQ-Me solutions increased with rising zinc concentration in the presence of Ca^{2+} and Mg^{2+}. The compounds STQ-Et and STQ-CF_3 demonstrated either weak divalent cation selectivity or very poor stability and a tendency to aggregate in saline. Fluorescence measurements of living KB cells incubated with ZnO NPs and stained with STQ-Me showed a pattern similar to that of the well-known fluorescent zinc indicator TSQ. However, STQ-Me was most likely not able to chelate protein-bound zinc, as evidenced by the dynamic fluorescence parameters of KB cells. Thus, STQ-Me has the potential for use in measuring zinc in living cells, but the molecular design requires modification to enhance fluorescence and expand its ability to chelate protein-bound zinc.

Declarations

Funding

This publication received financial support from the Ministry of Education and Science of Ukraine project “Polymer systems and nanocomposites for optoelectronics” (grant no. 0124U001177).

Ethics and Consent to Participate declarations

Not applicable.

Author Contributions Statement

Pavlo V.: Investigations, Methodology, Formal analysis, Writing – Original Draft Preparation, Writing – Review & Editing;

S. S.: Writing – Review & Editing, Formal analysis;

Petro V.: Investigations, Methodology, Writing – Review & Editing;

N. K.: Conceptualization, Formal analysis, Writing – Review & Editing;

O. K.: Writing – Review & Editing, Visualization;

V. S.: Investigations, Methodology, Conceptualization, Writing – Original Draft Preparation, Writing – Review & Editing.

All authors reviewed the manuscript.

Competing interests policy

The authors declare no competing interests.

Dual publication

Results/data/figures in submission have not been previously published

Authorship

The authors confirm have read the journal policies and is submitting their manuscript in accordance with those policies.

Permission to Use Third-Party Materials

Third-party materials were not used in the preparation of the manuscript.

Data Availability

The data will be available on request.

References

1. Li F, Li Y, Wang Y, Chen X, Liu X, Cui J. Association between magnesium depletion score and the risk of metabolic dysfunction associated steatotic liver disease: a cross sectional study. Sci Rep. 2024;14(1):24627. https://doi.org/10.1038/s41598-024-75274-8.
2. Stiles LI, Ferrao K, Mehta KJ. Role of zinc in health and disease. Clin experimental Med. 2024;24(1):38. https://doi.org/10.1007/s10238-024-01302-6.
3. Fiorentini D, Cappadone C, Farruggia G, Prata C. Magnesium: Biochemistry, Nutrition, Detection, and Social Impact of Diseases Linked to Its Deficiency. Nutrients. 2021;13(4):1136. https://doi.org/10.3390/nu13041136.
4. Baracaldo-Santamaría D, Avendaño-Lopez SS, Ariza-Salamanca DF, Rodriguez-Giraldo M, Calderon-Ospina CA, González-Reyes RE, Nava-Mesa MO. Role of Calcium Modulation in the Pathophysiology and Treatment of Alzheimer's Disease. Int J Mol Sci. 2023;24(10):9067. https://doi.org/10.3390/ijms24109067.
5. Petersen OH, Gerasimenko JV, Gerasimenko OV, Gryshchenko O, Peng S. The roles of calcium and ATP in the physiology and pathology of the exocrine pancreas. Physiol Rev. 2021;101(4):1691–744. https://doi.org/10.1152/physrev.00003.2021.
6. Tangvoraphonkchai K, Davenport A. Magnesium and Cardiovascular Disease. Adv Chronic Kidney Dis. 2018;25(3):251–60. https://doi.org/10.1053/j.ackd.2018.02.010.
7. Touyz RM, de Baaij JHF, Hoenderop JGJ. Magnesium Disorders. N Engl J Med. 2024;390(21):1998–2009. https://doi.org/10.1056/NEJMra1510603.
8. Matikainen N, Pekkarinen T, Ryhänen EM, Schalin-Jäntti C. Physiology of Calcium Homeostasis: An Overview. Endocrinol Metab Clin North Am. 2021;50(4):575–90. https://doi.org/10.1016/j.ecl.2021.07.005.

9. Chen B, Yu P, Chan WN, Xie F, Zhang Y, Liang L, Leung KT, Lo KW, Yu J, Tse GMK, Kang W, To KF. Cellular zinc metabolism and zinc signaling: from biological functions to diseases and therapeutic targets. Signal Transduct Target therapy. 2024;9(1):6. https://doi.org/10.1038/s41392-023-01679-y.
10. Sypniewska M, Pokladko-Kowar M, Gondek E, Apostoluk A, Kamedulski P, Smokal V, Song P, Liu J, Szczesny R, Derkowska-Zielinska B. Organic LEDs Based on Bis(8-hydroxyquinoline) Zinc Derivatives with a Styryl Group. Molecules. 2023;28(21):7435. https://doi.org/10.3390/molecules28217435.
11. Bissani GC, Pilger DA. 8-Hydroxyquinoline, Derivatives and Metal-Complexes: A Review of Antileukemia Activities. ChemistrySelect. 2023;8:e202204219. https://doi.org/10.1002/slct.202204219.
12. Wang Y, Li D, Xu K, Wang G, Zhang F. Copper homeostasis and neurodegenerative diseases. Neural regeneration Res. 2025;20(11):3124–43. https://doi.org/10.4103/NRR.NRR-D-24-00642.
13. Ferreira LM, García-García P, García PA, Castro MA. A review on quinolines: New green synthetic methods and bioactive potential. Eur J Pharm Sci. 2025;209:107097. https://doi.org/10.1016/j.ejps.2025.107097.
14. Ferreira LM, García-García P, García PA, Castro MÁ. A review on quinolines: New green synthetic methods and bioactive potential. Eur J Pharm Sci. 2025;209:107097. https://doi.org/10.1016/j.ejps.2025.107097.
15. Rigo GV, Joaquim AR, Macedo AJ, de Andrade SF, Tasca T. Iron chelation and inhibition of metallopeptidases mediate anti-Trichomonas vaginalis activity by a novel 8-hydroxyquinoline derivative. Bioorg Chem. 2022;125:105912. https://doi.org/10.1016/j.bioorg.2022.105912.
16. Du LQ, Zeng CJ, Mo DY, Qin QP, Tan MX, Liang H. 8-hydroxyquinoline-N-oxide copper(II)- and zinc(II)-phenanthroline and bipyridine coordination compounds: Design, synthesis, structures, and antitumor evaluation. J Inorg Biochem. 2024;251:112443. https://doi.org/10.1016/j.jinorgbio.2023.112443.
17. Seo H, Jackl MK, Kalaj M, Cohen SM. Developing Metal-Binding Isosteres of 8-Hydroxyquinoline as Metalloenzyme Inhibitor Scaffolds. Inorg Chem. 2022;61(19):7631–41. https://doi.org/10.1021/acs.inorgchem.2c00891.
18. Rohini, Paul K, Luxami V. 8-Hydroxyquinoline Fluorophore for Sensing of Metal Ions and Anions. Chem Rec. 2020;20(12):1430–73. https://doi.org/10.1002/tcr.202000082.
19. Wang D, Li SJ, Cao W, Wang Z, Ma Y. ESIPT-Active 8-Hydroxyquinoline-Based Fluorescence Sensor for Zn(II) Detection and Aggregation-Induced Emission of the Zn(II) Complex. ACS omega. 2022;7(21):18017–26. https://doi.org/10.1021/acsomega.2c01414.
20. Olaleye SO, Idowu SO, Ahmed S, Khan MA. New 8-hydroxyquinoline-based azo dyes as highly sensitive colorimetric chemosensors for nickel cation. RSC Adv. 2025;15(5):3497–514. https://doi.org/10.1039/d4ra08510h.
21. Smokal V, Krupka A, Kharchenko O, Krupka O, Derkowska-Zielinska B, Kolendo A. Synthesis and photophysical properties of new styrylquinoline-containing polymers. Mol Cryst Liq Cryst. 2018;661(1):38–44. https://doi.org/10.1080/15421406.2018.1460236.

22. Chumachenko V, Virych P, Nie G, Virych P, Yeshchenko O, Khort P, Tkachenko A, Prokopiuk V, Lukianova N, Zadvornyi T, Rawiso M, Ding L, Kutsevol N. Combined Dextran-Graft-Polyacrylamide/Zinc Oxide Nanocarrier for Effective Anticancer Therapy in vitro. Int J Nanomed. 2023;18:4821–38. https://doi.org/10.2147/IJN.S416046.
23. Chumachenko V, Virych P, Nie G, Virych P, Yeshchenko O, Khort P, Tkachenko A, Prokopiuk V, Lukianova N, Zadvornyi T, Rawiso M, Ding L, Kutsevol N. Combined Dextran-Graft-Polyacrylamide/Zinc Oxide Nanocarrier for Effective Anticancer Therapy in vitro. Int J Nanomed. 2023;18:4821–38. https://doi.org/10.2147/IJN.S416046.
24. Virych P, Virych P, Prokopiuk V, Onishchenko A, Ischenko M, Doroschuk V, Kurovska V, Tkachenko A, Kutsevol N. Dextran-Graft-Polyacrylamide/Zinc Oxide Nanoparticles Inhibit of Cancer Cells in vitro and in vivo. Int J Nanomed. 2024;19:11719–43. https://doi.org/10.2147/IJN.S485106.
25. Hübner C, Keil C, Jürgensen A, Barthel L, Haase H. Comparison of Three Low-Molecular-Weight Fluorescent Probes for Measuring Free Zinc Levels in Cultured Mammary Cells. Nutrients. 2023;15(8):1873. https://doi.org/10.3390/nu15081873.
26. Prachayasittikul V, Prachayasittikul S, Ruchirawat S, Prachayasittikul V. 8-Hydroxyquinolines: a review of their metal chelating properties and medicinal applications. Drug Des Devel Ther. 2013;7:1157–78. https://doi.org/10.2147/DDDT.S49763.
27. Telbiz G, Leonenko E, Dvoynenko M. Optical properties of Rh6G molecules ordering in the silica- and titanium dioxide mesoscopic sol-gel films. Mol Cryst Liq Cryst. 2017;642:74–80. http://dx.doi.org/10.1080/15421406.2016.1255052.
28. Otsuki J. Supramolecular approach towards light-harvesting materials based on porphyrins and chlorophylls. J Mater Chem A. 2018;6:6710–53. https://doi.org/10.1039/C7TA11274B.
29. Hestand NJ, Spano FC. Expanded Theory of H- and J-Molecular Aggregates: The Effects of Vibronic Coupling and Intermolecular Charge Transfer. Chem Rev. 2018;118(15):7069–163. https://doi.org/10.1021/acs.chemrev.7b00581.
30. Hecht M, Wurthner F. Supramolecularly Engineered J-Aggregates Based on Perylene Bisimide Dyes. Acc Chem Res. 2021;54(3):642–53. https://doi.org/10.1021/acs.accounts.0c00590.
31. Ma S, Du S, Pan G, Dai S, Xu B, Tian W. Organic molecular aggregates: From aggregation structure to emission property. Aggregate. 2021;2:e96. https://doi.org/10.1002/agt2.96.
32. Bricks JL, Slominskii YL, Panas ID, Demchenko AP. Fluorescent J-aggregates of cyanine dyes: basic research and applications Review. Methods Appl Fluoresc. 2018;6(1):012001. https://doi.org/10.1088/2050-6120/aa8d0d.
33. Gao F. Photo-induced interaction of hydrophobic and hydrophilic dye molecules at nanometer distances. Dyes Pigm. 2002;52(3):223–30. https://doi.org/10.1016/s0143-7208(01)00084-5.
34. Wurthner F, Kaiser TE, Saha-Moller CR. J-Aggregates: From Serendipitous Discovery to Supramolecular Engineering of Functional Dye Materials. Angew Chem. 2011;50(15):3376–410. https://doi.org/10.1002/anie.201002307.

35. Park S, Ghosh P, Park S, Lee Y, Kwak S, Kwon O-H. Origin of ultraweak fluorescence of 8-hydroxyquinoline in water: photoinduced ultrafast proton transfer. RSC Adv. 2016;6:9812–21. https://doi.org/10.1039/C5RA23802A.
36. Yaermaimaiti G, An H, Kadir A, Rao X, Qin C, Abulimiti B, Xiang M. Investigation of the substituent effect on the excited- state intramolecular proton transfer of 8-hydroxyquinoline. Results Chem. 2024;7:101318. https://doi.org/10.1016/j.rechem.2024.101318.
37. Gupta R, Luxami V, Paul K. Insights of 8-hydroxyquinolines: A novel target in medicinal chemistry. Bioorg Chem. 2021;108:104633. https://doi.org/10.1016/j.bioorg.2021.104633.
38. Kohanfekr T, Gholamrezazadeh C, Hosseini HA. Vanadium 8-hydroxyquinoline derivatives in medicine: current state and future outlook. Biometals. 2025;38(3):711–36. https://doi.org/10.1007/s10534-025-00683-9.
39. Li BY, Yang F, Zhang ZY, Shen YF, Wang T, Zhao L, Qin JC, Ling F, Wang GX. Quinoline, with the active site of 8-hydroxyl, efficiently inhibits Micropterus salmoides rhabdovirus (MSRV) infection in vitro and in vivo. J Fish Dis. 2022;45(6):895–905. https://doi.org/10.1111/jfd.13615.
40. Li L, Wu H, Wang J, Ji Z, Fang T, Lu H, Yan L, Shen F, Zhang D, Jiang Y, Ni T. Discovery of Novel 8-Hydroxyquinoline Derivatives with Potent *In Vitro* and *In Vivo* Antifungal Activity. J Med Chem. 2023;66(23):16364–76. https://doi.org/10.1021/acs.jmedchem.3c01771.
41. Carrascosa E, Bull JN, Martínez-Núñez E, Scholz MS, Buntine JT, Bieske EJ. Photoisomerization of Linear and Stacked Isomers of a Charged Styryl Dye: A Tandem Ion Mobility Study. J Am Soc Mass Spectrom. 2021;32(12):2842–51. https://doi.org/10.1021/jasms.1c00264.
42. Sifain AE, Gifford BJ, Gao DW, Lystrom L, Nelson TR, Tretiak S. NEXMD Modeling of Photoisomerization Dynamics of 4-Styrylquinoline. J Phys Chem. 2018;122(49):9403–11. https://doi.org/10.1021/acs.jpca.8b09103.
43. Krupka O, Smokal V, Derkowska-Zielinska B, Kolendo A. Optical and Photochemical Properties of Diarylethylenes. Opt Mater Biomaterials Secur Def Syst Technol XIV. 2017;10440:C104400–1. https://doi.org/10.1117/12.2278118.
44. Shiraishi Y, Ichimura C, Sumiya S, Hirai T. Multicolor Fluorescence of a Styrylquinoline Dye Tuned by Metal Cations. Chem – Eur J. 2011;17:8324–32. https://doi.org/10.1002/chem.201101048.
45. Meeusen JW, Tomasiewicz H, Nowakowski A, Petering DH. TSQ (6-methoxy-8-p-toluenesulfonamido-quinoline), a common fluorescent sensor for cellular zinc, images zinc proteins. Inorg Chem. 2011;50(16):7563–73. https://doi.org/10.1021/ic200478q.

Figures

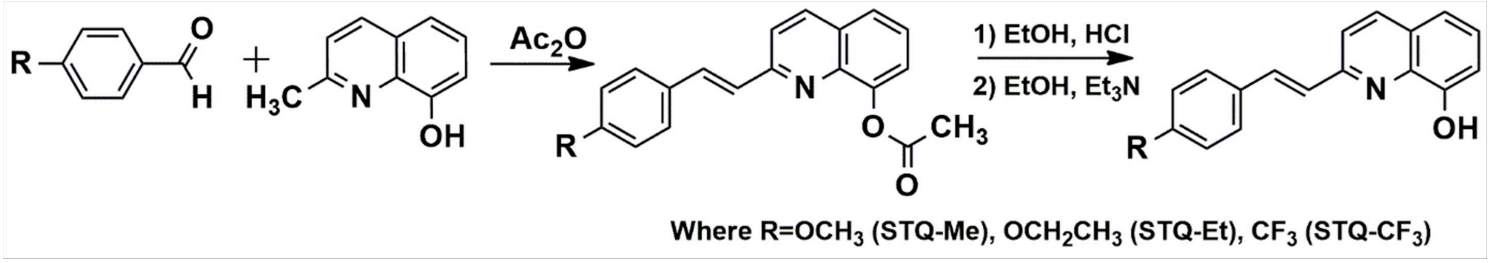

Figure 1

Synthesis of quinoline containing derivatives.

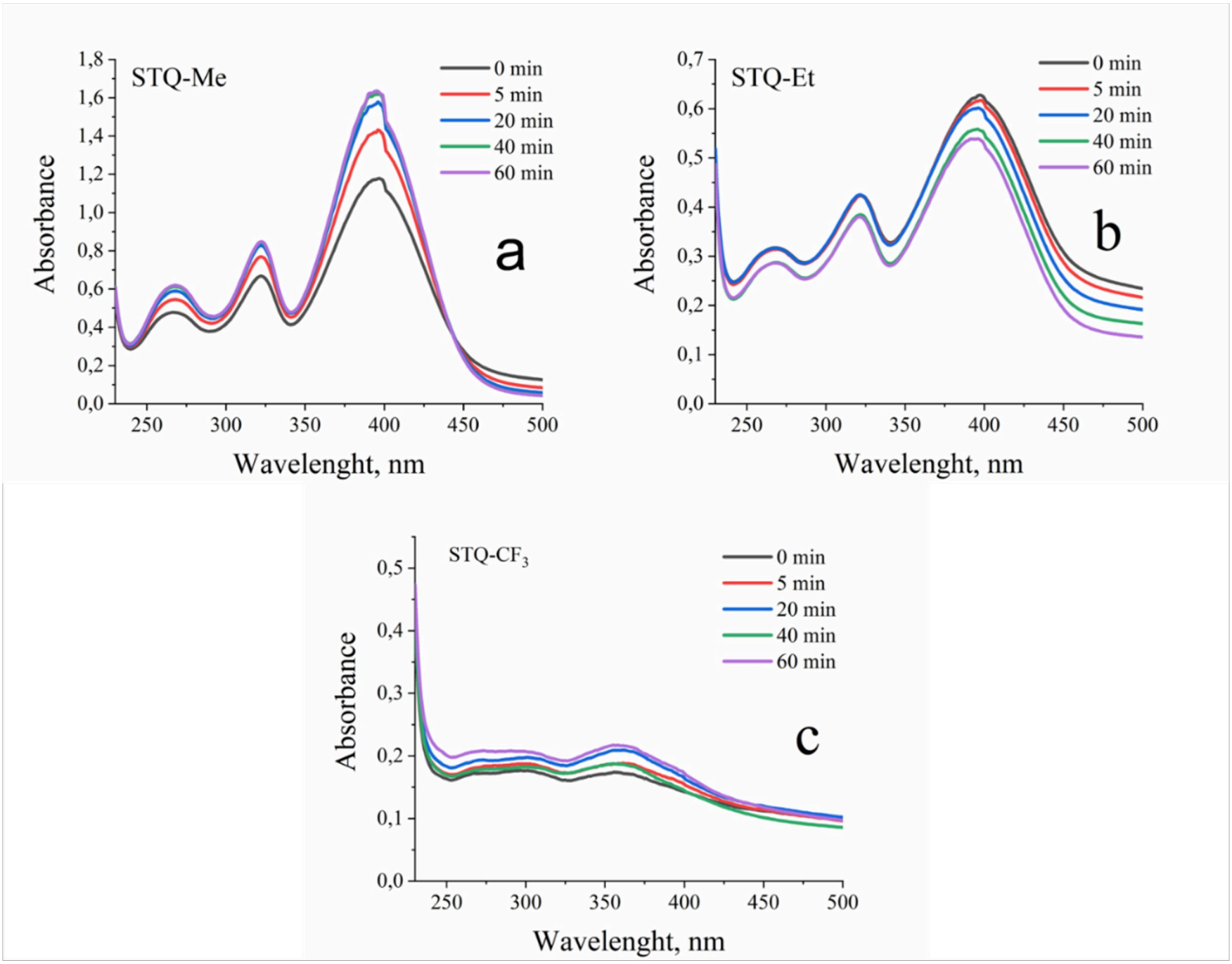

Figure 2

Changes in the absorbance spectra of 50 μM solutions of STQ-Me, STQ-Et and STQ-CF_3 in saline over 60 min.

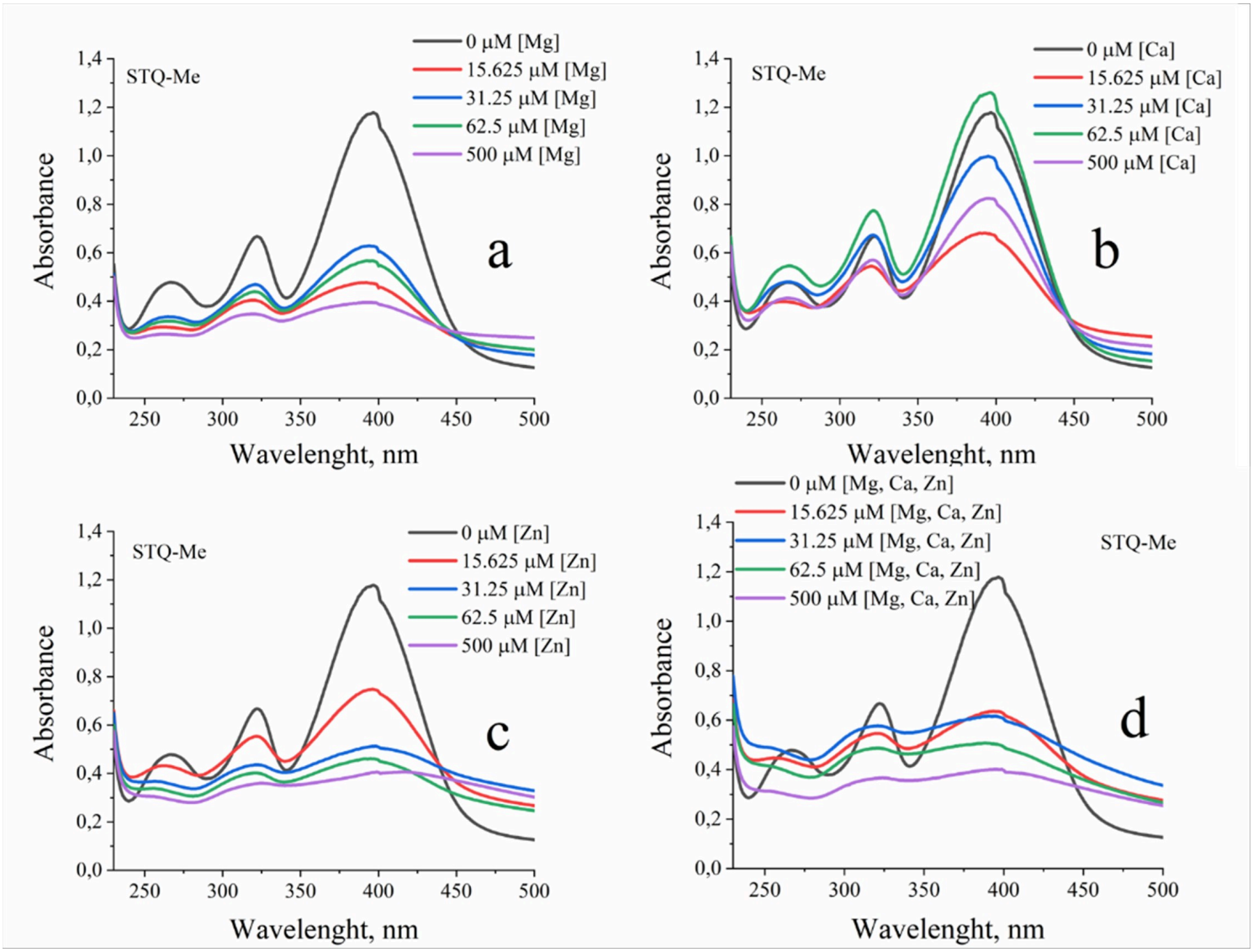

Figure 3

Absorbance of STQ-Me (50 µM) in saline solution with Mg^{2+} (a), Ca^{2+} (b), Zn^{2+} (c) and mix (d) of these cations with the same concentration of each (C = 15.625 µM, 31.25 µM, 62.5 µM and 500 µM). Spectra were measured after 5 min of incubation.

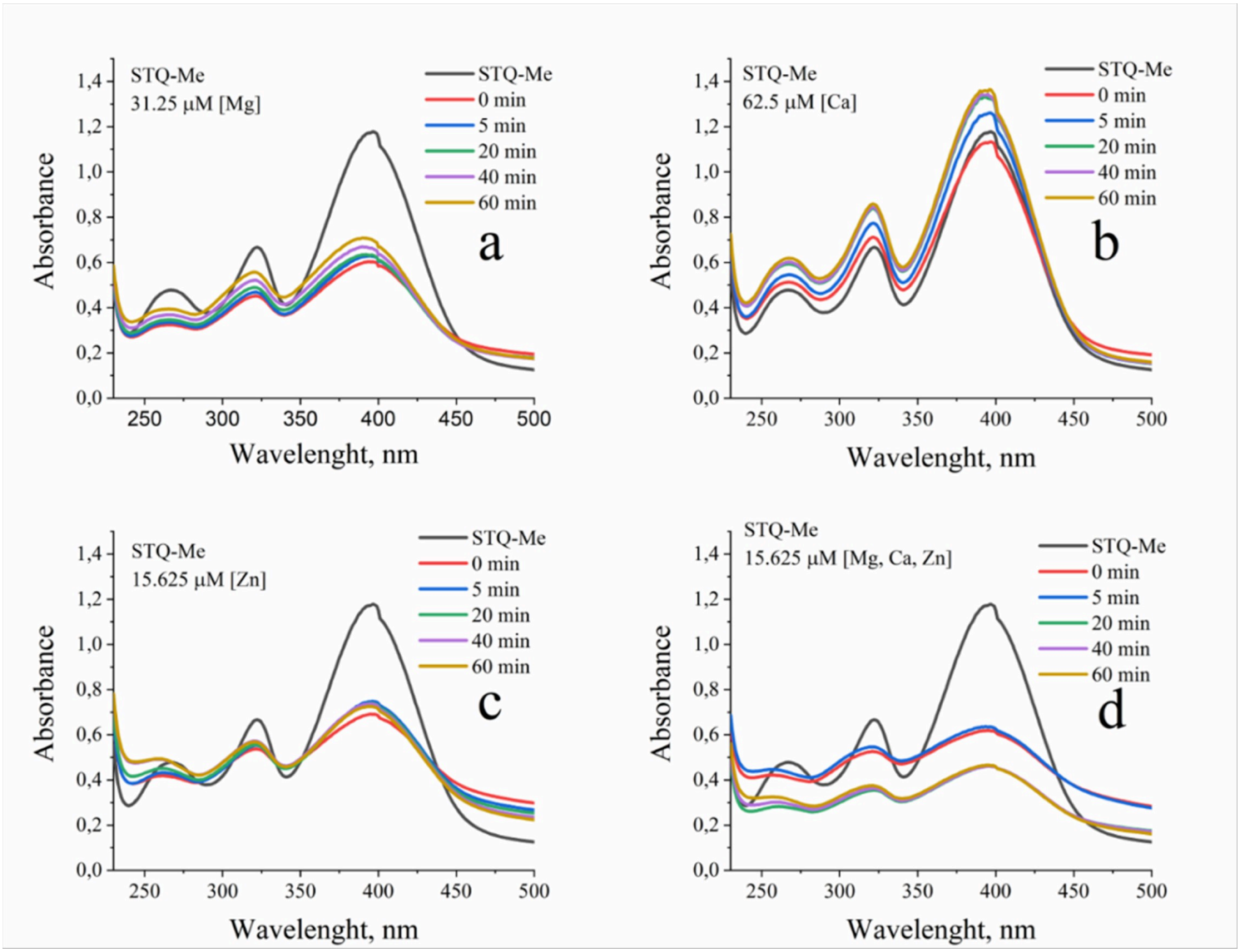

Figure 4

Absorbance of STQ-Me (50 µM) in saline solution with C = Mg^{2+} 31.25 µM (a), Ca^{2+} 62.5 µM (b), Zn^{2+} 15.625 µM (c) and 15.625 µM mix of each cation (d). Spectra were measured after 0 min, 5 min, 20 min, 40 min and 60 min of incubation

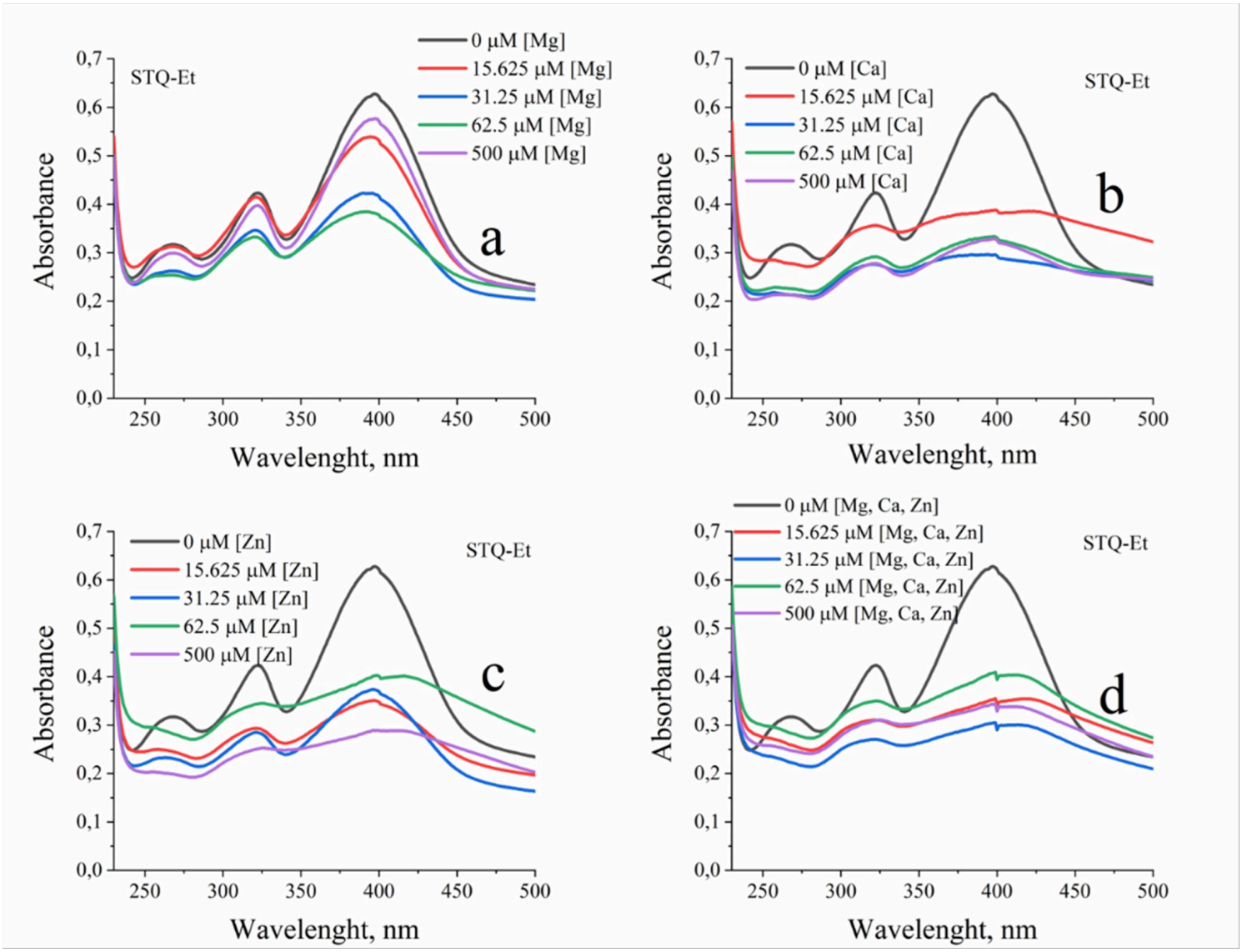

Figure 5

Absorbance of of STQ-Et (50 µM) in saline solution with Mg^{2+} (a), Ca^{2+} (b), Zn^{2+} (c) and mix (d) of these cations with the same concentration of each (C = 15.625 µM, 31.25 µM, 62.5 µM and 500 µM). Spectra were measured after 5 min of incubation.

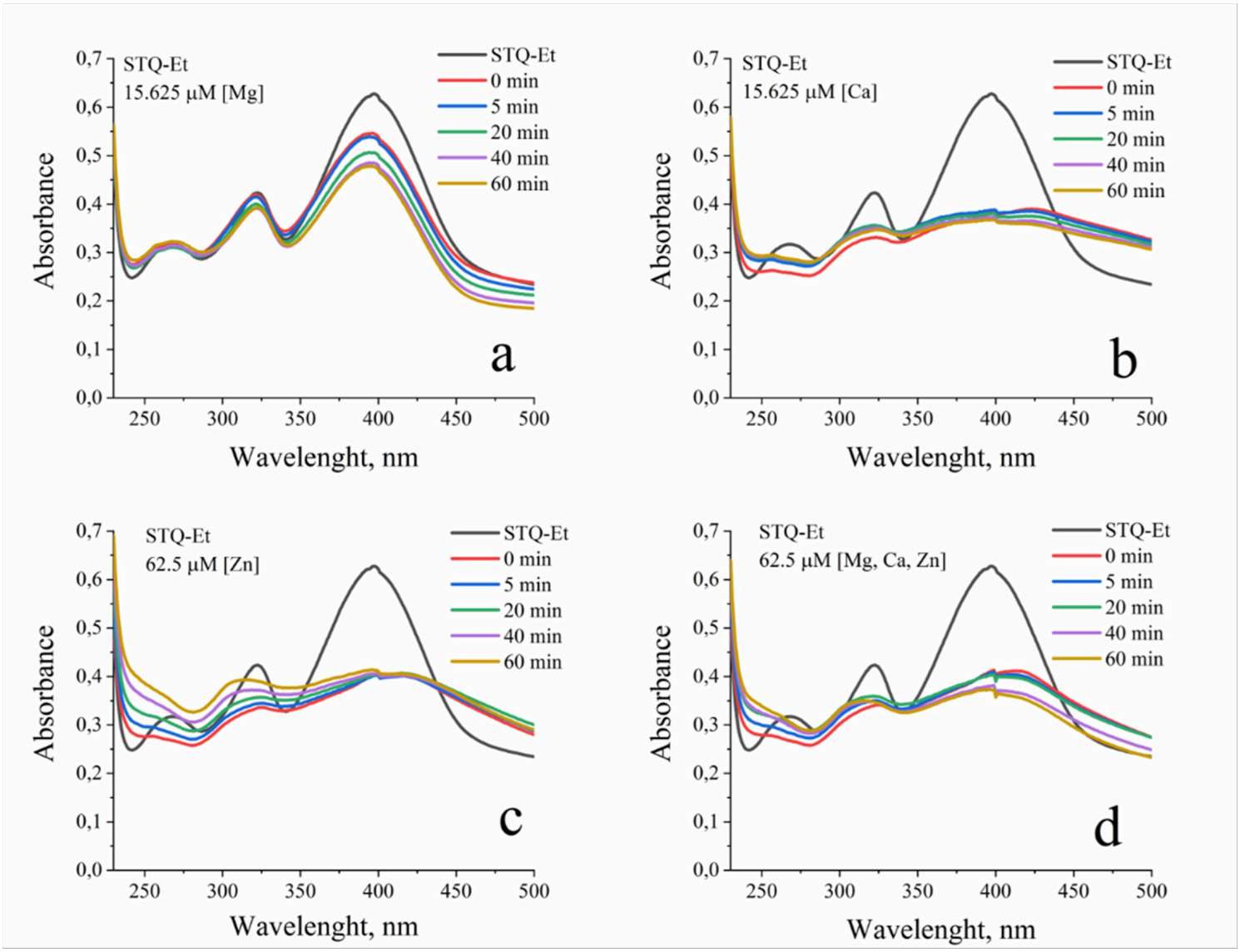

Figure 6

Absorbance of STQ-Et (50 µM) in saline solution with C = Mg^{2+} 15.625 µM (a), Ca^{2+} 15.625 µM (b), Zn^{2+} 62.5 µM (c) and 62.5 µM mix of each cation (d). Spectra were measured after 0 min, 5 min, 20 min, 40 min and 60 min of incubation.

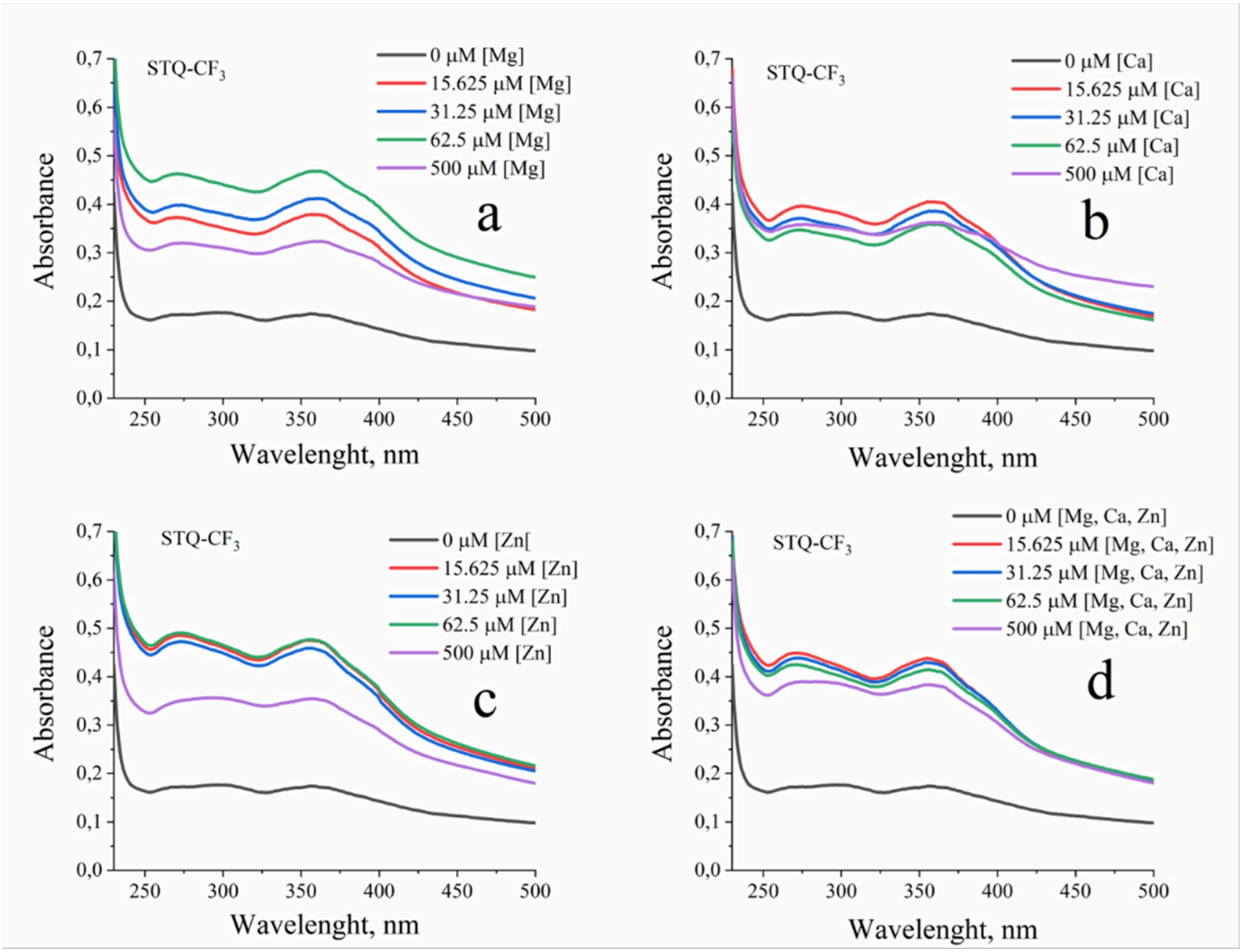

Figure 7

Absorbance of STQ-CF_3 (50 µM) in saline solution with Mg^{2+} (a), Ca^{2+} (b), Zn^{2+} (c) and mix (d) of these cations with the same concentration of each (C = 15.625 µM, 31.25 µM, 62.5 µM and 500 µM). Spectra were measured after 5 min of incubation.

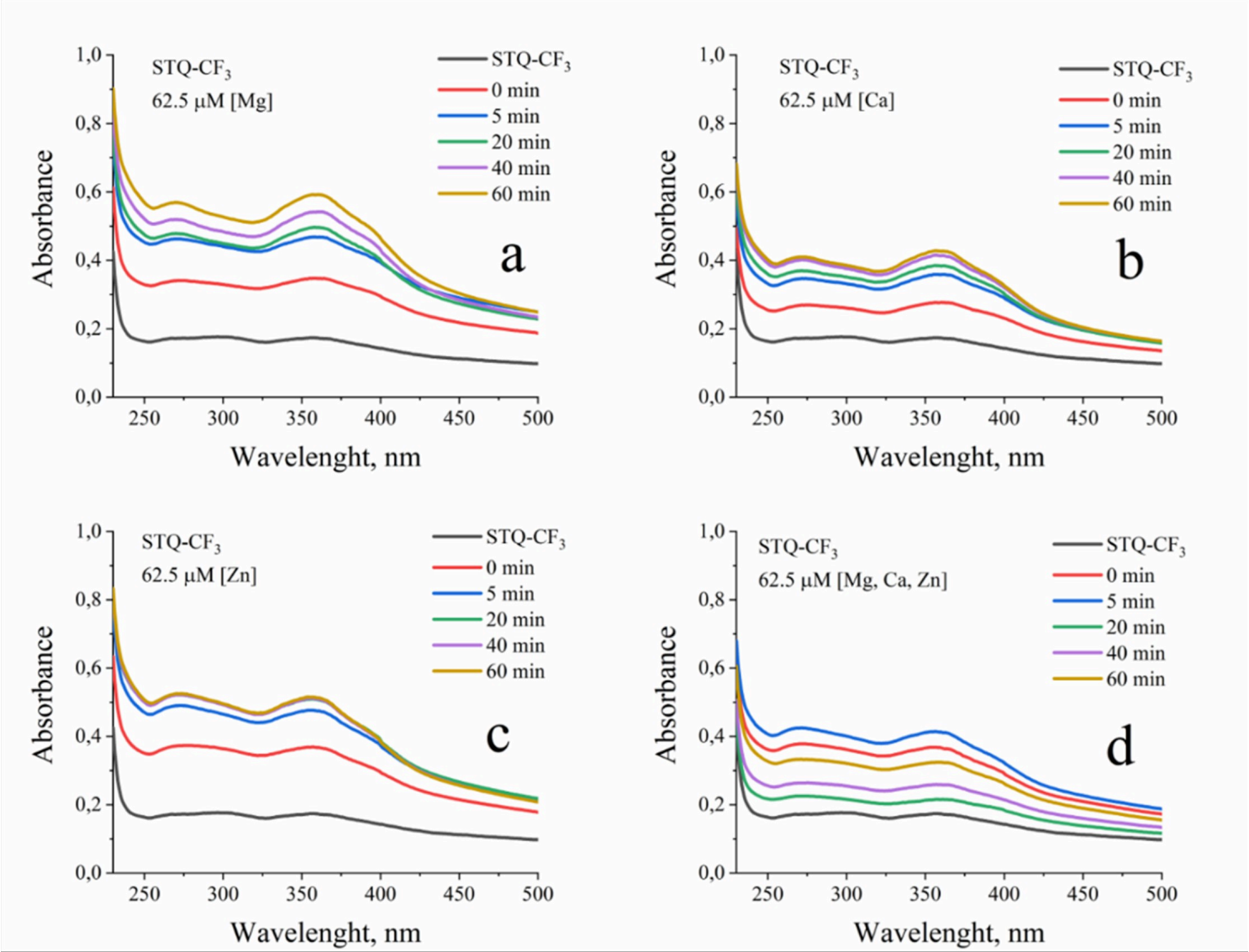

Figure 8

Absorbance of STQ-CF_3 (50 µM) in saline solution with C = Mg^{2+} 62.5 µM (a), Ca^{2+} 62.5 µM (b), Zn^{2+} 62.5 µM (c) and 62.5 µM mix of each cation (d). Spectra were measured after 0 min, 5 min, 20 min, 40 min and 60 min of incubation.

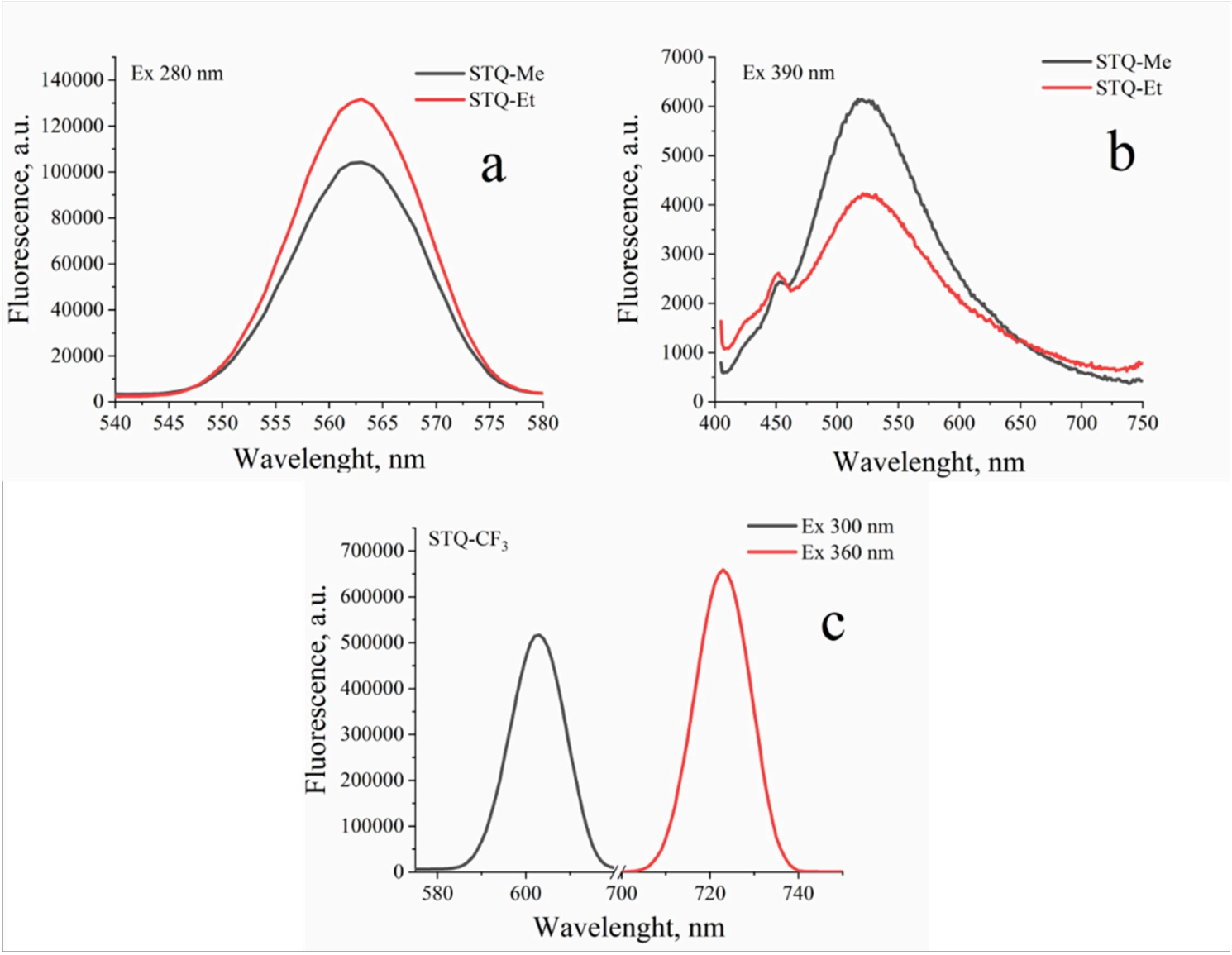

Figure 9

Fluorescence spectra of 50 μM STQ-Me (a), STQ-Et (b) and STQ-CF_3 (c) in saline solutions after 40 min of incubation (l_{ex} 280 nm, 390 nm for STQ-Me and STQ-Et; 300 nm, 360 nm for STQ-CF_3).

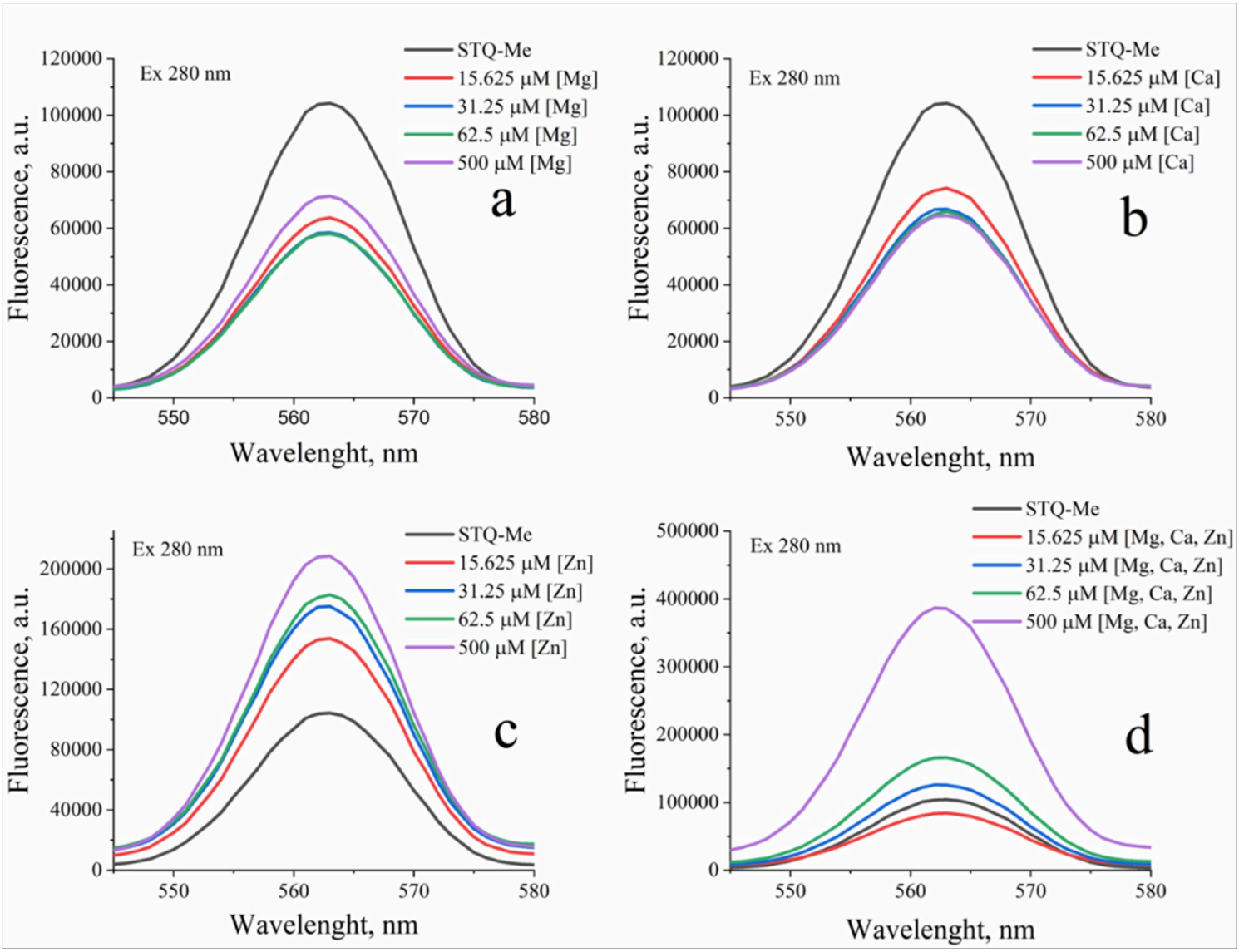

Figure 10

Fluorescence of STQ-Me (50 µM) in saline solution with Mg^{2+} (a), Ca^{2+} (b), Zn^{2+} (c) and mix (d) of these cations with the same concentration of each (C = 15.625 µM, 31.25 µM, 62.5 µM and 500 µM), after 40 min of incubation (l_{ex} 280 nm).

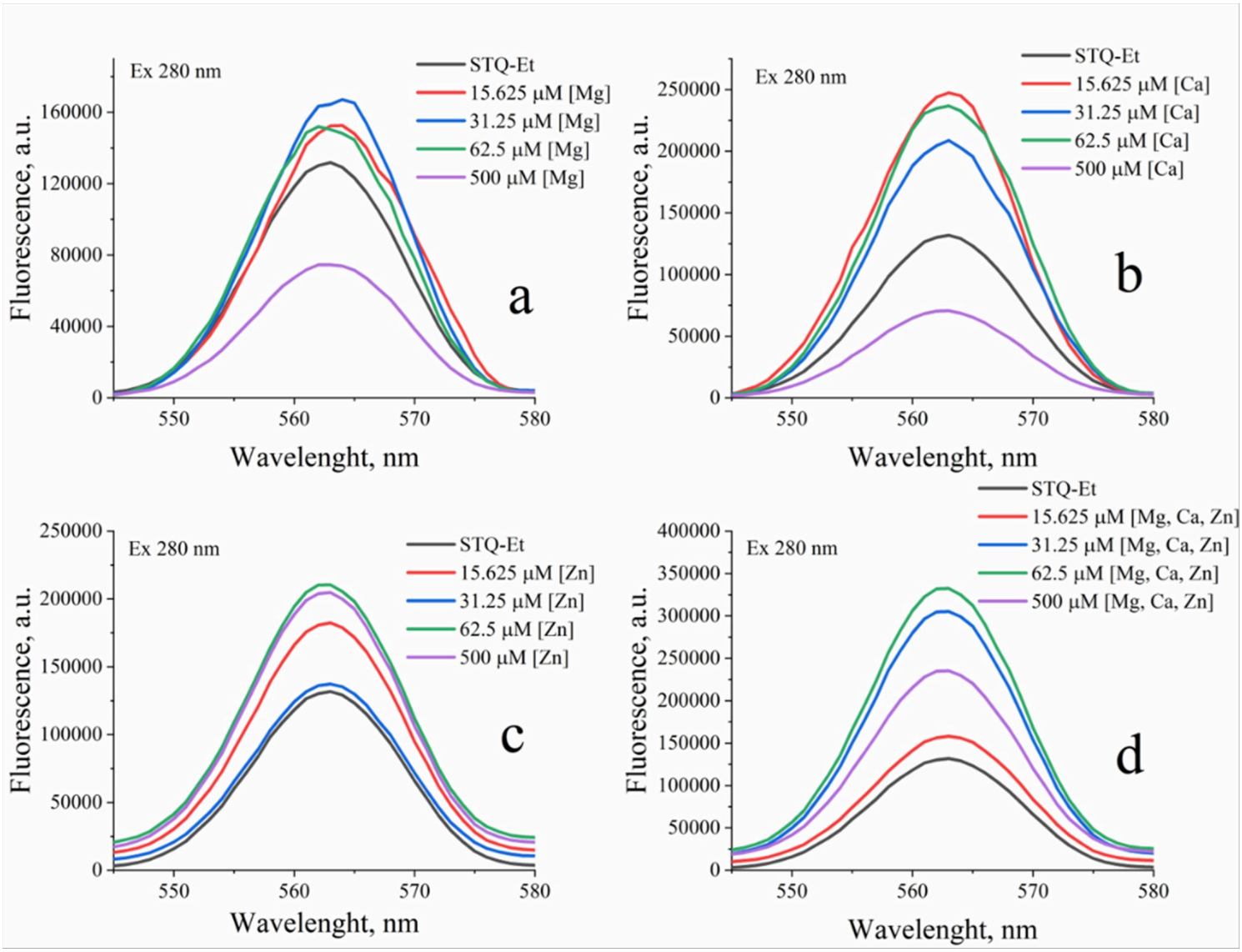

Figure 11

Fluorescence of STQ-Et (50 µM) in saline solution with Mg^{2+} (a), Ca^{2+} (b), Zn^{2+} (c) and mix (d) of these cations with the same concentration of each (C = 15.625 µM, 31.25 µM, 62.5 µM and 500 µM), after 40 min of incubation (l_{ex} 280 nm).

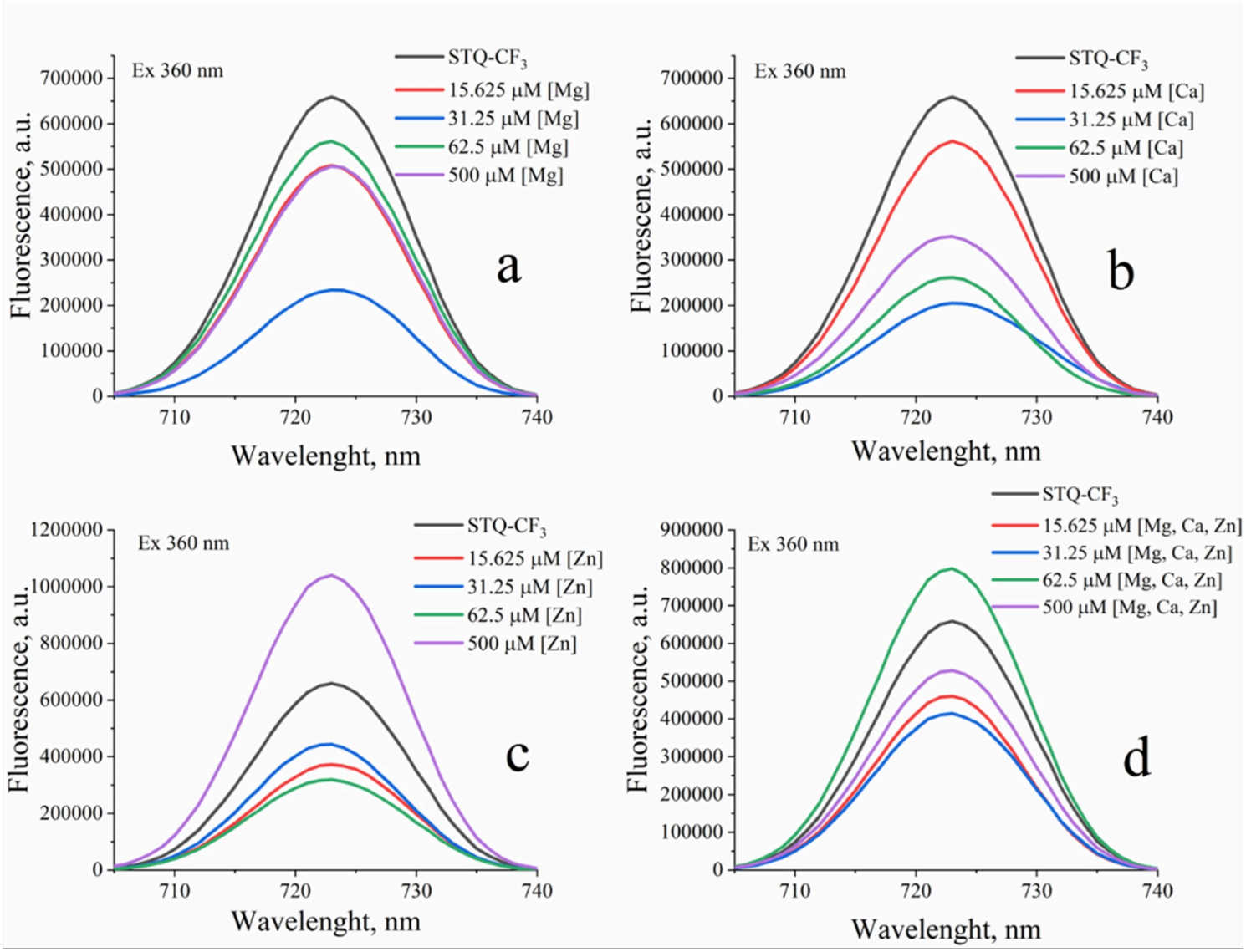

Figure 12

Fluorescence of STQ-CF_3 (50 µM) in saline solution with Mg^{2+} (a), Ca^{2+} (b), Zn^{2+} (c) and mix (d) of these cations with the same concentration of each (C = 15.625 µM, 31.25 µM, 62.5 µM and 500 µM), after 40 min of incubation (Ex wavelength 280 nm).

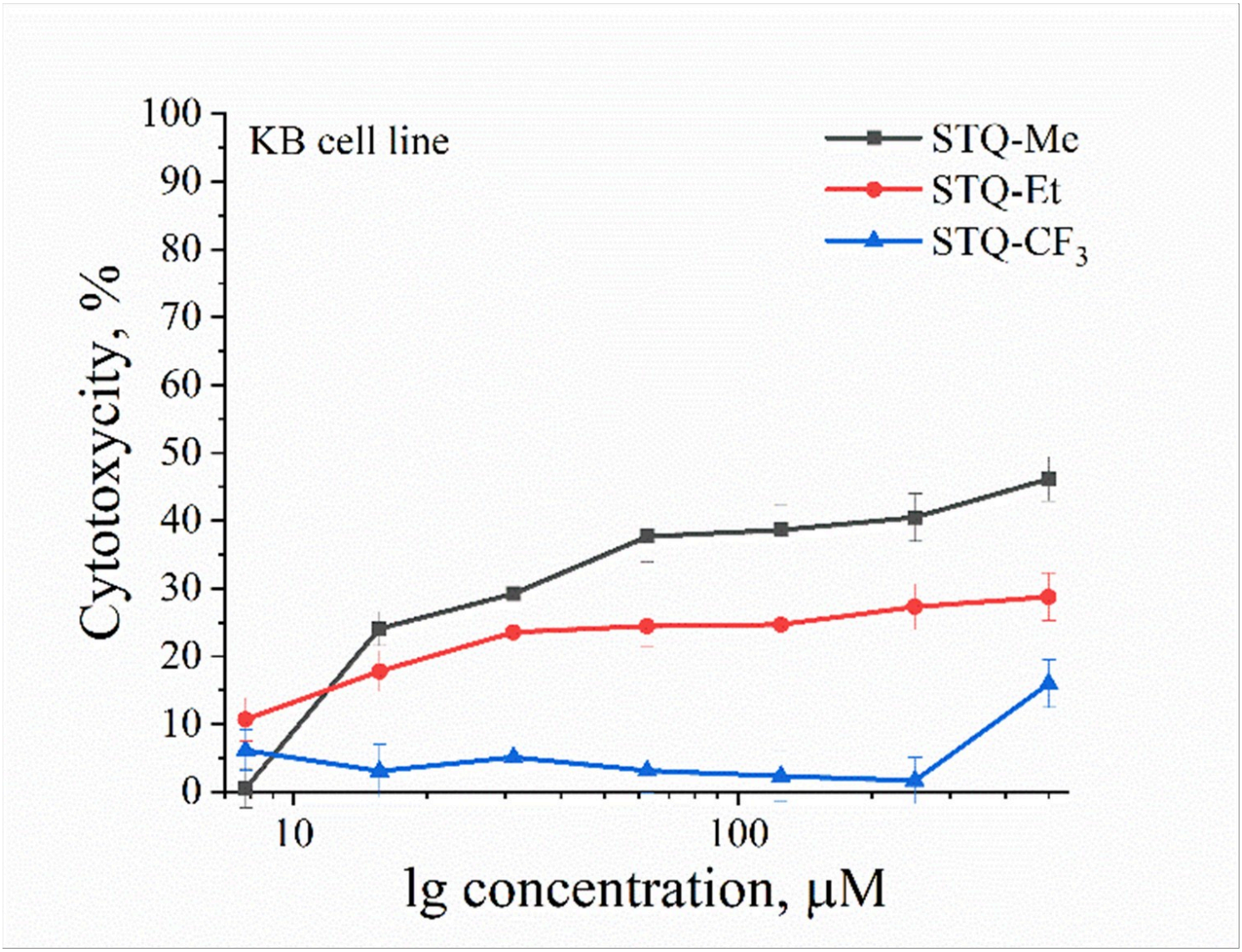

Figure 13

Survival of mouth epidermal carcinoma cell line KB treated by STQ-Me, STQ-Et, STQ-CF_3 (n=4, M±SD).

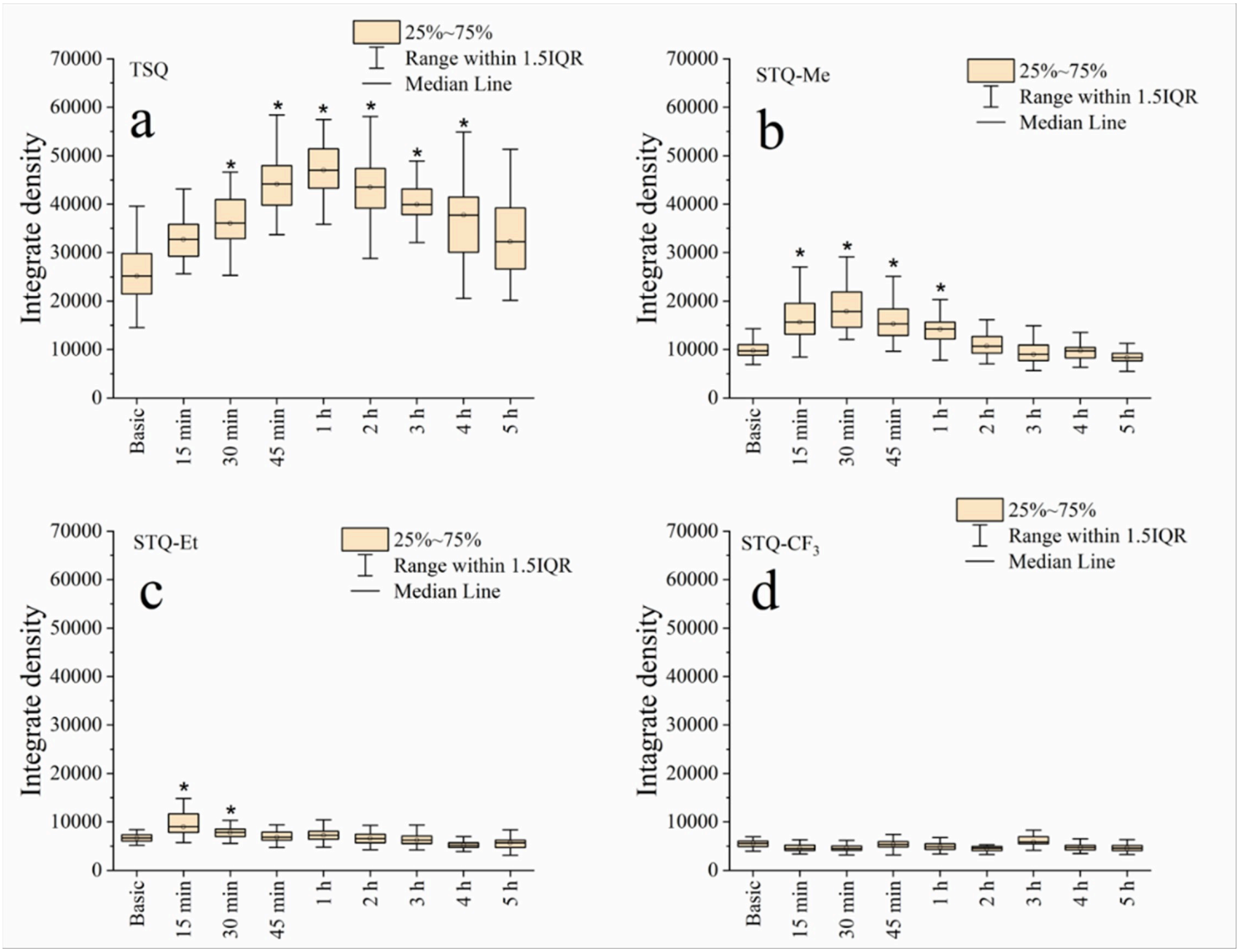

Figure 14

Fluorescence of KB cell line during their incubation with dextran-graft-polyacrylamide/ZnO nanoparticles (D-PAA/ZnO NPs) for 5 h (median, 25-75%; Kruskal-Wallis test: *p < 0.05 relative basic fluorescence). Staining with 30 μM TSQ (a) STQ-Me (b), STQ-Et (c) and STQ-CF_3 (d) for 30 min.

Supplementary Files

This is a list of supplementary files associated with this preprint. Click to download.

- Supplementaryinformation23.12.pdf
- floatimage1.jpeg